HHS Public Access

Author manuscript

Nat Rev Clin Oncol. Author manuscript; available in PMC 2015 October 01.

Published in final edited form as:

Nat Rev Clin Oncol. 2014 October ; 11(10): 566–584. doi:10.1038/nrclinonc.2014.126.

Vessel calibre—a potential MRI biomarker of tumour response in clinical trials

Kyrre E. Emblem, **Christian T. Farrar**, **Elizabeth R. Gerstner**, **Tracy T. Batchelor**, **Ronald J. H. Borra**, **Bruce R. Rosen**, **A. Gregory Sorensen**, and **Rakesh K. Jain**

The Intervention Centre, Oslo University Hospital, Sognsvannsveien 20, 0372 Oslo, Norway (K.E.E.). Department of Radiology and Athinoula A. Martinos Center for Biomedical Imaging, Massachusetts General Hospital and Harvard Medical School, Charlestown, MA 02129, USA (C.T.F., R.J.H.B., B.R.R.). Department of Neurology (E.R.G., T.T.B.), Edwin L. Steele Laboratory of Tumor Biology, Department of Radiation Oncology (R.K.J.), Massachusetts General Hospital and Harvard Medical School, 100 Blossom Street, Boston, MA 02114, USA. Siemens Healthcare Health Services, 51 Valley Stream Parkway, Malvern, PA 19355, USA (A.G.S.).

Abstract

Our understanding of the importance of blood vessels and angiogenesis in cancer has increased considerably over the past decades, and the assessment of tumour vessel calibre and structure has become increasingly important for *in vivo* monitoring of therapeutic response. The preferred method for *in vivo* imaging of most solid cancers is MRI, and the concept of vessel-calibre MRI has evolved since its initial inception in the early 1990s. Almost a quarter of a century later, unlike traditional contrast-enhanced MRI techniques, vessel-calibre MRI remains widely inaccessible to the general clinical community. The narrow availability of the technique is, in part, attributable to limited awareness and a lack of imaging standardization. Thus, the role of vessel-calibre MRI in early phase clinical trials remains to be determined. By contrast, regulatory approvals of antiangiogenic agents that are not directly cytotoxic have created an urgent need for clinical trials incorporating advanced imaging analyses, going beyond traditional assessments of tumour volume. To this end, we review the field of vessel-calibre MRI and summarize the emerging evidence supporting the use of this technique to monitor response to anticancer therapy. We also discuss the potential use of this biomarker assessment in clinical imaging trials and highlight relevant avenues for future research.

Correspondence to: K.E.E. kyrre@nmr.mgh.harvard.edu.

Competing interests

C.T.F., E.R.G. and R.J.H.B. declare no competing interests.

Author contributions

All authors made substantial contributions to researching data, discussion of content, writing, and review/editing of the manuscript before submission.

Supplementary information is linked to the online version of the paper at www.nature.com/nrclinonc.

Introduction

An abnormal vasculature characterized by disorganized, permeable and dilated vessels is a hallmark of cancer tissue.[1,2] Unlike the ordered microcirculatory arrangement of blood vessels found in normal tissue, the heterogeneous tumour vascular bed comprises a chaotic network of mixed vessel types, from small-calibre, capillary-like vessels to oversized and permeable post-capillary venule-like vessels, and vascular malformations. The formation of vessels with a wide spectrum of calibres—that is, the cross-sectional width of the vessel—in cancer tissue is attributed to compression of the vessel walls by tumour and host cells, as well as vessel dilatation owing to imbalance between proangiogenic and antiangiogenic factors.[3–7] The formation and development of abnormal tumour vessels have pivotal roles in the progression of cancers towards metastatic phenotypes and in determining the success of anticancer therapy.[5,8] Whereas contrast-enhanced MRI is generally considered the gold standard clinical approach for *in vivo* radiographic imaging assessment of the structural and haemodynamic status of solid tumours,[9] vessel-calibre MRI has emerged as a potentially useful approach for clinical trial response monitoring only over the past decade and is not widely established. With the advent of antivascular and antiangiogenic therapies that seem to be cytostatic rather than predominantly cytotoxic and, therefore, do not simply result in decreased tumour sizes, traditional assessment of radiographic response and progression-free survival according to MRI-based tumour-volume criteria can no longer be considered an adequate biomarker of therapeutic response.[9–15]

Herein, we provide a comprehensive and critical review of vessel-calibre assessment by MRI. We present a historical overview, ranging from the early development of this approach to current clinical trials, and explain the basic concepts underlying the technique. We summarize the proangiogenic and antiangiogenic influences that determine the structure of tumour vasculature, and explain how blood vessels can be imaged *in vivo* using MRI protocols. In addition, we discuss potential reasons for the lack of uptake of this methodology, and provide recommendations for imaging that we believe will enable realization of the full potential of vessel calibre as a biomarker in clinical trials. Finally, we highlight key advancements and future directions relating to vessel-calibre MRI.

Vessel calibres in solid cancers

The processes of tumour vascularization and growth, angiogenic pathways and targeted therapies are among the most-studied facets of cancer,[5,16–19] and a detailed description of these aspects is outside the scope of this Review. Nevertheless, we provide a brief overview of the relevant mechanisms that directly affect tumour-vessel calibres in the following sections.

The vasculature of solid cancers

For a tumour to grow beyond a few millimeters in diameter, the formation and remodelling of new blood vessels is essential.[16] Growth of the tumour vasculature is thought to occur in a variety of ways that includes: use of the pre-existing host vasculature (vessel co-option); growth of new vessels as branches from existing vessels (sprouting angiogenesis); splitting of existing blood vessels to form new branches (intussusception); *de novo* formation of

blood vessels independent of existing vessels, either comprising endothelial cells (vasculogenesis) or tumour cells in the absence of endothelial cells and fibroblasts (vascular mimicry); and transdifferentiation of tumour cells into endothelial cells.[5] Initially, many tumours grow by vessel co-option; however, at some point an angiogenic switch occurs that leads to overproduction of proangiogenic factors, such as vascular endothelial growth factor (VEGF), fibroblast growth factors (FGFs), angiopoietin-2 (ANG-2) and chemokines, which in turn leads to new vessel formation and vessel maturation (Figure 1).[1,5,17] The new vessels are predominantly immature and abnormal (overdilated, hyperpermeable, tortuous and disrupted), resulting in variable perfusion;[2,7] some tumour tissues receive too much blood, whereas others do not receive enough and are, therefore, starved of oxygen and nutrients.[2,7] In parallel, solid stress imparted by proliferating cancer cells, stromal cells and the extracellular matrix can lead to compression of vessels, reducing blood flow (Figure 1).[3,4,20,21] Consequently, the tumour vascular bed is spatially and temporally heterogeneous with regard to multiple vessel parameters, not least vessel calibre, which creates an irregular microenvironment that adversely affects drug delivery and introduces variation in cellular responses to therapeutic agents, resulting in decreased efficacy of cancer therapy.[8] Indeed, this microenvironment is characterized by hypoxia (low oxygen concentration),[22,23] low pH, increased solid stress[4,20] and high interstitial fluid pressure[24]—factors that can all contribute to tumour progression and resistance to various treatments (such as radiotherapy, chemotherapy and immunotherapy).[8,21]

Cancer therapies that affect vessel calibres

Treatments for cancer not only affect cancer cells, but also have broader effects on the tumour microenvironment, including the vasculature. Following radiation treatment, oxygen-deprived tumour tissue might become reoxygenated owing to radiation-induced death of surrounding radiosensitive and oxygen-rich cell populations that were previously obstructing nearby tumour blood vessels.[5] This alteration in the microvascular environment could potentially lead to decompression of tumour vessels, increased vessel calibres and increased perfusion of tumour tissues.[23] In addition, some chemotherapeutic drugs might kill proliferating endothelial cells and, therefore, act as antiangiogenic agents,[17] with the possible consequence of modifying blood-vessel calibres. Clearly, distinguishing treatment-related changes in tumour-vessel calibres from the alterations induced by tumour growth is important for patient management and clinical trial design.

Blocking angiogenesis was initially proposed as a strategy to starve tumours of blood flow and halt the delivery of nutrients required for cell survival, growth and proliferation.[25] However, the therapeutic potential of antiangiogenic agents also seems to be attributable to mechanisms other than simple destruction and ‘pruning’ of the tumour vasculature;[8] Jain and colleagues[1,26,27] have proposed that antiangiogenic agents can transiently normalize the tumour vasculature, converting the heterogeneous, abnormally dilated and hyperpermeable vessels to a more-efficient state that results in improved blood perfusion and decreased vessel diameters. This effect might create a window of opportunity during which various concomitantly administered therapies (radiation, chemotherapy or immunotherapy, for example) are likely to be most effective.[27,28] Additionally, antiangiogenic therapy could potentially disrupt the vascular cancer-stem-cell niche.[17] Probably, a range of mechanisms

are in fact operative at different time periods during antiangiogenic therapy; thus, the proposed diverse mechanisms of action are unlikely to be mutually exclusive.[17,29]

Challenges to antiangiogenic therapy

Heterogeneity within an individual tumour, as well as among and across cancer types, suggests that each tumour responds differently to therapies depending on the biology of the component cancer-cell populations and their microenvironment.[6] As is true for cancer-cell-directed therapies, some tumours are intrinsically resistant and others develop resistance to antiangiogenic therapies.[5,18] Tumours can develop resistance by upregulating distinct compensatory proangiogenic pathways that can circumvent therapy, or might continue to grow because of the seeming inability of the antiangiogenic agent to prune established blood vessels. Both of these possibilities highlight the need for direct measurements of vascular response—or lack thereof.

Furthermore, studies of a number of anti-VEGF agents have highlighted the importance of dosing regimens tailored to individual tumours and time-dependent drug scheduling.[28] Whereas low doses of anti-VEGF agents might induce vascular normalization and improve the delivery of adjuvant therapies, high doses might result in an excessive decrease in the number of functional tumour blood vessel pathways and, therefore, compromise drug delivery.[8] For example, in patients with non-small-cell lung cancer, tumour perfusion and the net influx rate of docetaxel, a taxane targeting the microtubular network, were reduced within 5 h after administration of a 15 mg/kg dose of the anti-VEGF antibody bevacizumab.[30] A lower dose of bevacizumab might have had the opposite effect according to the concept of vascular normalization, although this possibility remains to be proven in patients. In two mouse models of breast cancer,[31] low doses (5 mg/kg) of an anti-VEGFR2 antibody, DC101, increased perfusion of nanoparticles, whereas a higher dose (10 mg/kg) seemed to hinder tumour perfusion. Similarly, the size of the concomitantly administered therapeutic agent also seemed to be important in this study; the lower dose of DC101 was shown to reduce vessel diameters and improved the permeability of the tumour to 12 nm particles, but not 60 nm or 125 nm particles.[31] Furthermore, the therapeutic efficacy of albumin-bound paclitaxel (nab-paclitaxel), which is around 10 nm in size, was increased by DC101 treatment, whereas the outcome of therapy with doxil, which is approximately 100 nm in size, was not affected by this anti-VEGF agent; doxil and nab-paclitaxel had similar efficacy in the absence of DC101 therapy. These results suggest that selected doses of DC101 can induce a vascular normalization effect that increases tumour perfusion, but only to smaller molecules, possibly by creating a more homogeneous vasculature, but with smaller vessel—or ‘pore’—diameters. In addition, a preclinical study of bevacizumab in mouse xenograft models of human ovarian and oesophageal cancers demonstrated decreased tumour uptake of trastuzumab and bevacizumab antibodies, and human immunoglobulin G, as well as reduced *ex vivo* mean vessel densities.[32] Thus, the dose of bevacizumab used in this study might have resulted in ‘pruning’ of too many blood vessels and caused a decrease in the size of vascular pores, owing to increased pericyte coverage, to below that of an antibody.[31] Together, these findings provide additional evidence of the gaps in our knowledge relating to the vascular responses to anticancer therapies that necessitate the development of assessments of vascular outcomes.

The dose-dependence of antiangiogenic agents has implications not only for conventional chemotherapeutics and low-molecular-weight targeted therapies, but also for the delivery of nanotherapeutics. Tumour blood vessels are more permeable to large molecules than many normal vessels, which provides an intriguing mechanism for selective delivery of macromolecules to tumours.[33] Moreover, large molecules are retained within tumours because of poor clearance by impaired lymphatic systems. These concepts are collectively known as enhanced permeability and retention (EPR).[34–37] Successful outcomes of EPR-based nanotherapeutics will probably—similarly to conventional therapies—be governed by the tumour type as well as the dose and timing of concurrent antiangiogenic therapies.[35] Furthermore, because the extracellular matrix can also retard the penetration of nanotherapeutics in tumours,[38] improved delivery of nanoparticles might require normalization of both tumour vessel and the extracellular matrix.[8] Thus, vessel-calibre MRI might be equally important in optimizing and monitoring such approaches.

Traditional MRI in cancer therapy

Conventional MRI in monitoring response

Current approach—Use of conventional MRI for monitoring response to therapy in solid tumours has been reviewed extensively.[11,12,14,15] In short, most aggressive pathological lesions are easily identified using T_1-weighted MRI protocols after administration of a standard gadolinium-based contrast agent, on the basis of the increased vascularity and permeability of tumour vessels. T_1-weighted images are sensitized to the longitudinal magnetic-relaxation time of protons in water molecules (T_1), and paramagnetic contrast agents, such as gadolinium, increase the MRI signal intensity in the blood by shortening the T_1-relaxation times. These images are usually complemented by T_2-weighted MRI, fluid-attenuated inversion recovery (FLAIR) MRI (Figure 2) and diffusion-weighted MRI for assessments of peritumoural oedema and changes in cellular density.[39,40] Traditional T_2-weighted images are sensitive to local inhomogeneity of the magnetic field, a phenomenon known as the 'magnetic susceptibility effect',[41] which describes the tendency of fat, water and fluids to produce hyperintense signals whereas blood appears dark (hypointense). Definitions of the most-common terminologies used in vessel-calibre MRI are provided in Supplementary Table 1 online.

Formalized imaging-based response criteria are usually based on the Response Evaluation Criteria in Solid Tumors (RECIST) guidelines[42]—a National Cancer Institute (NCI)-funded initiative—that are applicable to data derived from MRI, CT and most other modalities used for noninvasive *in vivo* imaging. The aim of the RECIST criteria is to provide simple and objective measures of therapeutic response based on assessment of the post-treatment change (or lack of change) in the longest in-plane diameters of target lesions located throughout the body (Supplementary Table 2). A slightly different approach is used for the evaluation of tumours in the CNS, termed the MacDonald criteria,[43] which focus on indicators of response related to the extent (area) of contrast enhancement on imaging, corticosteroid dose, and clinical status. In 2010, the MacDonald criteria were updated by the Response Assessment in Neuro-Oncology (RANO) working group[11] to include changes in the non-enhancing lesion on FLAIR MRI; however, the definition of increased FLAIR

hyperintensity is subjective and was not clearly defined in these guidelines (Supplementary Table 2), leading to variability in application of the RANO criteria.

Limitations of the current approach—The RECIST and RANO working groups acknowledged the inherent limitations associated with imaging-based response criteria focusing on tumour size alone;[42,44–46] nevertheless, these criteria, which predominantly rely on radiographic measures of the response of tumours to therapy, are frequently criticized.[47–49] The controversy surrounding these guidelines includes debate over the definition of true radiographic response and whether response criteria should be based solely on anatomical tumour load or in conjunction with metrics that better reflect vascular or metabolic changes in the tumour.[47,50,51] In particular, the dynamic nature of the perfusion of vascularized lesions cannot be characterized accurately using traditional measurements of contrast-agent-induced signal enhancement alone,[9] whereas potential monitoring of the EPR effect will require quantitative measures of the permeability rate-constant.[35] Moreover, not all cancer types are expected to follow similar definitions of response; for example, obtaining repeated measurements in adherence with the RECIST criteria is difficult for localized or locally recurrent cancers of the prostate because of the location and small size of such tumours, whereas increased levels of prostate-specific antigen (PSA) are closely correlated with imminent radiographic progression and are, therefore, used widely as the preferred indicator of tumour status.[52] Whether the RECIST criteria reflect a meaningful end point of response to many specific antiangiogenic therapies also remains unclear. For example, although sunitinib treatment in hepatocellular carcinoma seems to cause tumour necrosis or cysts, no subsequent tumour shrinkage was observed in one study.[53]

Furthermore, manually defined response criteria that are dependent solely on tumour size are prone to reader bias attributable to inconsistencies in the interpretation of irregular tumour edges, regional variations in contrast enhancement within surgical cavities and permeability changes resulting from radiotherapy and antiangiogenic therapy, as well as the lack of consensus in the type and dose of contrast agent used.[12,54,55] In addition, variations in positioning of the patient's head in the scanner between examinations can have a substantial influence on the reader's assessment of the data. Indeed, repeated assessment of therapeutic response using the RANO criteria was shown to return an intra-reader error rate of 22%, which might have resulted in patients without true tumour progression being incorrectly identified as having progressive disease, and could potentially have led to discontinuation of treatment or their removal from a clinical trial.[56]

A transient, therapy-induced increase in radiographic oedema and contrast enhancement following radiotherapy, termed 'pseudoprogression', has been the cause of much research and debate, especially in relation to brain tumours.[57] Radiotherapy has a profound effect on tumour blood-vessel morphology, inducing vasodilation, increased vascular permeability and oedema,[57,58] that can resemble radiographic characteristics of tumour progression. However, unlike true disease progression, pseudoprogression is typically associated with reversion of MRI indications of tumour progression after a few weeks or months without any change in therapy. Of note, up to 30% of patients with intra-axial brain tumours show signs of pseudoprogression,[11,57] and distinguishing these treatment-related changes from active tumour growth is critically important for patient management and the administration

of clinical trials. By contrast, blockade of VEGF using antiangiogenic therapies can result in reduced tumour-vessel permeability and vasogenic oedema that enhances radiographic-response rates, but, unfortunately, this improvement does not always translate into increased survival.[13,45] Thus, an urgent need exists, particularly in the setting of antivascular and antiangiogenic clinical trials, for validated methods and standards for assessment of tumour vascular structure and function beyond the current conventional MRI modalities.[59–62]

Perfusion MRI

Perfusion MRI can help address the issues relating to tumour vascularity and conflicting treatment effects observed with conventional MRI. A large number of early phase clinical trials have reported values of blood flow, blood volume, and permeability determined using perfusion MRI (recently reviewed in this journal[9] and elsewhere[63,64]). However, these data are beyond the scope of this Review, and we provide only a brief overview of relevance of this technique to vessel-calibre MRI.

Perfusion imaging techniques are based on the central volume principle,[65] which states that in a closed flow system with a single inflow orifice and a single outflow orifice, the blood volume of a given tissue is equal to the constant rate of blood flow (volume of blood in tissue per unit time) multiplied by the mean transit time of the blood tracer (that is, the MRI contrast agent) passing through the capillary structure of the tissue. Two main contrast agent-based perfusion MRI techniques are available, depending on whether the acquisition is made using T_1-sensitive or T_2-sensitive imaging protocols.[66] In T_1-weighted perfusion MRI, the signal intensity increases dynamically as a function of the local concentration of contrast agent; this technique is primarily used for estimating vessel permeability and is generally referred to as dynamic contrast-enhanced (DCE)-MRI. Alternatively, a T_2-weighted perfusion MRI sequence is used for accurate measures of blood-flow rate, blood volume and vessel calibre following a rapid, intravenous injection of contrast agent. More specifically, rapid echo-planar imaging techniques, which enable imaging of the entire volume of interest within a few seconds, are typically employed. Using this approach, a decrease in the dynamic MRI signal intensity is observed following injection of contrast agent, as the echo-planar imaging technique is particularly sensitive to the magnetic susceptibility effect (Figure 2b). Consequently, this imaging technique is referred to as dynamic susceptibility contrast (DSC)-MRI (Supplementary Methods).

Vessel-calibre MRI

Basic concepts

In 1991, Fisel, Rosen and colleagues[67–69] at Massachusetts General Hospital, Boston, USA, pioneered the theoretical foundation for the vessel-calibre MRI technique. In a series of studies,[67–69] these researchers used Monte Carlo simulations to provide evidence that T_2-weighted perfusion MRI images were sensitive to the vessel-size-related scale of the magnetic susceptibility effect created by blood and contrast agents flowing through vessels. This initial work was performed in conjunction with substantial efforts to understand MRI signal alterations resulting from changes in oxyhaemoglobin concentrations in blood.[70,71] These initiatives were followed by comprehensive models for quantification of magnetic

susceptibility effects *in vivo*.[72–76] The first image representative of the use of the vessel-calibre technique in cancer, specifically a rat C6 glioma xenograft model, was reported in 1998 by Dennie and collegues.[77] 19 days after cell implantation, the gliomas showed evidence of a 90% increase in the average vessel diameter compared with adjacent normal grey matter. The first clinical experience of this technique was reported in 2000 by Donahue and colleagues, who published vessel-calibre images of 15 patients with intracranial tumours; a positive correlation between average vessel calibres and tumour grade was also demonstrated.[78]

Although vessel-calibre MRI was conceptualized >20 years ago and can provide a direct link between tumour vascular status and therapeutic response,[5] the technique has received limited attention in the literature on perfusion MRI.[9,63,66,79–81] One important reason for this apparent deficit is the complex image acquisition process used in vessel-calibre MRI, which has hindered the technique from becoming readily accessible to the general clinical community.[59] The methodology necessitates the acquisition of images using both gradient-echo and spin-echo protocols (Figure 2b). This approach enables relative (unitless) measures of average vessel diameters and average vessel densities for arteries, capillaries, and veins combined to be estimated in each image pixel using the quotient of gradient-echo blood volumes to spin-echo blood volumes (Box 1).[82] Efforts have also been made to quantify the average vessel calibre in an image voxel (in μm), which is often referred to as the vessel size index (VSI), using a weighted average of vessel calibres and accounting for water diffusion and the absolute blood volume fraction.[82–85] These measurements are possible because of the high sensitivity of the gradient-echo sequence to the magnetic susceptibility effect in both small (radius <10 μm) and large (radius >10 μm) vessel calibres, whereas the spin-echo sequence has an extra imaging component that minimizes the magnetic susceptibility effect for large-calibre vessels and is, therefore, selectively sensitive to detection of small calibre vessels (Supplementary Methods).[73,74] Henceforth, for simplicity, the gradient-echo images will be referred to as ‘macrovessel’ (also referred to as total blood volume[86,87]) images and the spin-echo images as ‘microvessel’ images.

Currently, three distinctly different analytical approaches to vessel-calibre MRI have been described, each having dedicated imaging protocols, caveats and postprocessing routines (Table 1). Firstly, a common approach is the direct assessment of the point-by-point difference in the macrovessel and microvessel DSC-MRI signal-intensity curves following injection of a low-molecular-weight (hydrodynamic diameter of <10 nm) gadolinium-based contrast agent (Figure 2c).[73–75,77,88,89] Secondly, vessel calibres can be estimated from macrovessel and microvessel imaging readouts before and after injection of super-paramagnetic iron-oxide (SPIO) nanoparticles, which are particularly useful in evaluating permeable cancer blood vessels outside the CNS.[77,85,90,91] Because most ultrasmall superparamagnetic iron-oxide molecules have diameters of approximately 30 nm,[92] SPIO-based agents are restricted to the intravascular space and might, therefore, more accurately reflect the average vessel calibre compared with contrast agents that leak out from the intravascular to the extravascular space (such as gadolinium-based agents). The relative long half-life of SPIO-based agents (up to approximately 24 hours)[92] also increases the image signal-to-noise ratio.[93] Finally, vessel-calibre MRI in the brain can also be acquired without

the use of contrast agents, simply by stimulating the blood-oxygen-level-dependent (BOLD) effect in both macrovessel and microvessel images (so-called BOLD-VSI; Supplementary Methods).[70,94,95] Compared with baseline signal intensities, image contrast is attributable to a change in the level of deoxygenated blood from brain activation stimuli or by normoxic or carbogen gas challenges. As this approach relies on the assessment of deoxygenated blood volume fractions, the method can provide a measure of apparent tissue oxygenation levels,[96] but is inherently limited to measures of venous vessel calibres.[95]

Because vessel calibres can be estimated from macrovessel and microvessel MRI before and after injection of a tracer, or by BOLD-VSI, the vessel-calibre technique can be readily implemented in the clinic using commonly available sequences.[83,97] Alternatively, for a combined simultaneous macrovessel–microvessel DSC-MRI readout,[89] most if not all major manufacturers of MRI apparatus provide dedicated image protocols upon request through their research and development programmes.

Assumptions underlying the calibre estimates

Vessel-calibre MRI is performed according to certain assumptions that in most clinical scenarios hold true. However, a few considerations specific to estimating vessel calibre in tumours need to be highlighted (Table 1).[85]

First, as noted by Troprès and colleagues in 2001,[83] reliable average VSI estimations (in μm) are difficult to obtain and must be interpreted with care, appreciating the complex relationships between macrovessel and microvessel blood volume and diffusion. A correct proportionality constant that accurately scales the MRI-based vessel-calibre estimate with the true vessel calibre and tissue blood volume is not currently available.[84,98] Also, owing to the additional influence of the relaxation rate of deoxygenated blood on the T_2 relaxation rate and signal intensities, the relationship between tissue oxygenation and the absolute vessel-calibre estimate is not straightforward in pathological conditions with impaired oxygen saturation levels, and warrants further investigations in the context of cancer therapy.[73,99] The accuracy of the VSI estimate should, however, improve with the use of higher magnetic-field strengths (>3 Tesla [3T]) and of dedicated ultrafast MRI measures of the arterial inflow,[100] and as better approximations of the relationship between the MRI signal and true blood volume values are established.[83,94] Thus, the current clinical hardware and imaging protocols limit the traditional VSI estimate to vessel radii considered larger than ‘very small’ (>2 μm) but smaller than ‘very large’ (<50 μm).[94,101,102] The range of vessel calibres that can be acceptably defined using BOLD-VSI is probably even narrower because of the inherent small changes in magnetic susceptibility during activation of the target tissue.[94]

Second, SPIO-based agents[90,103] are currently restricted to off-label use and should be applied with care because they have been associated with adverse effects, including allergic reactions, back pain and, in some extreme cases, cardiovascular events.[104,105] Although good agreement (r^2 ~0.8–0.9) has been observed between gadolinium-based VSI and SPIO-based VSI estimates, similarly high agreements might not be seen in direct comparisons of the macrovessel and microvessel parameter values obtained using the two agents owing to differences in the image acquisition protocols (Table 1).[106]

Third, unlike intravascular SPIO agents, gadolinium leaks out of the blood vessels into the interstitium, necessitating permeability compensation. Such compensation can be achieved using time-accelerated imaging techniques combined with multiple macrovessel image readouts,[85,107] preloading of a small gadolinium dose[106,108] or by rigorous post-processing corrections of the DSC-MRI signal curves (Supplementary Methods).[109–111]

Finally, whereas contrast-agent-based MRI vessel-calibre estimates typically provide values for static mean vessel calibres, Packard and colleagues used partial pressure of carbon dioxide ($PaCO_2$) challenges to show that tumours have decreased vascular reactivity, and that the native cerebral vasculature might also be dilated and constricted in response to transient or local changes in the $PaCO_2$.[86] BOLD-VSI analyses based on gas challenges is also influenced by vasodilation.[101] Increased cerebral vasodilation and flow is observed for hypercapnia (abnormally elevated CO_2 concentrations in the blood), whereas the opposite effect is seen in hypocapnia (low blood CO_2 levels);[112] however, the effects of gas-induced vasodilation on blood volume and, therefore, BOLD-VSI are not fully understood,[101] although venous volume fractions seem to be relatively unaffected by vasodilation.[113]

Validation of vessel-calibre MRI in cancer

Vessel-calibre MRI has been extensively validated against histology as well as other imaging modalities, such as *ex vivo* micro-CT and *in vivo* two-photon microscopy, to determine the value of MRI-based vessel-calibre measurements as a sensitive biomarker for cancer imaging (Supplementary Table 3). Absolute average MRI-determined vessel calibres tend to be slightly overestimated compared with histological vessel-calibre measurements, probably because of the incomplete understanding of the relationship between the blood MRI signal and the underlying physiology. Alternatively, the histological data might have been underestimated as a result of vessel collapse during cryosectioning (Supplementary Methods).[83,114] However, this differential between MRI and histological measurements seems to be relatively constant, with a subsequent strong correlation between the ratios of vessel calibres in tumour and reference tissue derived using each method (Table 2; Spearman correlation across all studies = 0.84; $P < 0.001$). Of note, comparison of *in vivo* imaging and *ex vivo* histological findings might also be compounded by geometrical differences and histological tissue distortions;[66] thus, not all studies performed to date have had the required sample size or objectives to statistically quantify comparisons of vessel-calibre estimates.

Several studies have shown excellent agreement between MRI and histological relative vessel calibres in C6, RG2 and U87 orthotopic glioma xenograft models.[77,91,115,116] Farrar and colleagues[91] also compared vessel-calibre MRI with *in vivo* two-photon microscopy measurements in separate tumour-size-matched groups of mice with U87 orthotopic gliomas, showing excellent agreement between the two techniques. Several studies of human breast cancer xenograft models have also found close correlations between MRI-determined vessel calibres and vessel calibres measured by *ex vivo* micro-CT,[117] immunohistology[118] and *in vivo* two-photon microscopy.[118] The validity of vessel-calibre MRI in mice bearing xenografts of poorly vascularized melanomas and highly vascular hemangioendotheliomas have been confirmed using both immunohistology and two-photon

microscopy.[118] In addition, Ungersma *et al.*[119] used a HM7 colorectal tumour model to demonstrate strong correlations between vessel calibres and between vessel densities determined using MRI, histology and micro-CT. Models of bone metastasis from breast cancer cell lines also show the same trend in MRI-derived and histological vessel calibres during antiangiogenic therapy.[120]

Collectively, these studies provide corroborating evidence that MRI-determined vessel calibres can serve as a surrogate marker of the microvasculature of cancers. Although a quantitative correction that enables accurate determination of physiologically correct vessel calibres by MRI is currently unavailable, reasonably accurate vessel-calibre ratios between tumour and normal tissue can be expected using this approach. Nevertheless, for vessel-calibre MRI and perfusion MRI to develop beyond expensive boutique methods, the true role and added value of these imaging techniques in clinical trials will remain unanswered until proper validation has been achieved in large, multicentre studies.[9,64,121]

Vessel-calibre MRI in human cancers

In keeping with the substantial increase in preclinical studies on vessel-calibre MRI over the past decade, the number of clinical studies is also increasing, providing data on vessel-calibre MRI in cancer, stroke and hypercapnia (Supplementary Figure 1, Supplementary Table 4). To date, vessel-calibre MRI studies in human cancers have focused on optimization of imaging and acquiring vessel-calibre measurements comparable to those in the literature (Table 3).

Clinical studies in CNS cancers—Unsurprisingly, considering the well-developed kinetic models for vascular tissue of the CNS,[122,123] the first human vessel-calibre MRI data in cancer were of intracranial tumours. The first images were published in 2000 by Donahue and co-workers.[78] These images were succeeded in 2004 by data from a corroborating study that included 72 patients with gliomas,[124] which demonstrated larger relative vessel calibres and a wider range of calibres with increasing tumour grade.[124] These findings have been confirmed in small glioma studies by Lamalle *et al.*[125] and by Hsu *et al.*[97] (n = 9 and 4, respectively), with larger vessel calibres and greater heterogeneity in vessel diameters in glioblastomas compared with lower grade gliomas. In parallel, Kiselev, Breyer, Xu and their colleagues[84,126–128] also presented supporting data from patients with brain lesions across several publications between 2003 to 2013; higher average MRI vessel calibres were reported in 20 intracerebral tumours (84 ± 73 μm) compared with adjacent white matter (32 ± 10 μm) and grey matter (34 ± 8 μm) tissue,[126] and a wider range of vessel calibres were observed in glioblastomas compared with lower grade gliomas.[84] These findings have also been confirmed in 31 patients at a higher clinical magnetic-field strength—3T, as opposed to 1.5T.[127]

At Massachusetts General Hospital, prior to administration of targeted therapies, abnormal and dilated vessel calibres were observed using MRI in a range of glioma grades,[129] recurrent glioblastomas[99,130,131] and newly diagnosed glioblastomas.[132] An almost threefold increase in average tumour-vessel calibres compared with whole-brain normal-appearing tissue was detected in 30 patients with recurrent glioblastomas (21 ± 6 μm versus

8 ± 1 μm),[99] and in two separate cohorts comprising 40 and 14 patients with newly diagnosed, untreated glioblastomas (24 ± 15 μm versus 8 ± 2 μm, and 33 ± 20 μm versus 11 ± 5 μm, respectively),[132] confirming the findings of Kiselev and colleagues.[126] Owing to refinements to the acquisition methods used in these studies,[99,132] including the use of a pre-dose injection of contrast agent to saturate the tissue and arterial input function normalization,[83,126] the absolute vessel-calibre values were lower compared with those reported by Kiselev *et al.*[126] Although this inconsistency emphasizes the need for caution when considering absolute vessel-calibre values (Table 1), data from the Massachusetts General Hospital show low intrapatient variations in MRI-derived tumour-vessel calibres.[133] The vessel calibres in normal-appearing tissue are also in good agreement with the findings of a study involving healthy volunteers and the use of an intravascular SPIO contrast agent (12–13 ± 2–3 μm).[93]

Clinical studies in non-CNS cancers—Lüdemann and colleagues[134] used MRI with a gadolinium-based contrast agent to compare vessel calibres in untreated prostate cancer tissue from 13 patients to peripheral normal-appearing tissue from the same patients, and observed a trend towards larger vessel diameters in tumour tissues; the prostate vasculature had heterogeneous signatures across patients, with a wide range of vessel diameters in tumours (112 ± 158 μm) and normal-appearing tissues (105 ± 205 μm).[134] The reproducibility of vessel-calibre MRI has also been evaluated in a pleomorphic sarcoma in the left pubic bone; stability over a 6-min acquisition window (4–5 μm) was high and, more importantly, vessel-calibre estimates were independent of dilution of the contrast agent.[85] Fredrickson *et al.*[103] successfully evaluated the feasibility of SPIO-based mean vessel density estimations using vessel-calibre MRI protocols (Box 1) in patients with colorectal liver metastases. Overall, the tracer kinetics of intravascular SPIO contrast agents and the subsequent uptake in the reticuloendothelial system of the liver and spleen over time does not seem to affect the vessel-calibre estimates in healthy and tumour tissues outside the CNS during the typical image acquisition period and at clinical magnetic-field strengths (≥1.5T).[85,106,135,136]

Vessel-calibre MRI in clinical trials

Lessons learnt from preclinical studies

Changes in vessel calibres determined using MRI compared with control or pretreatment values have been evaluated for a double-digit number of therapies in small rodent cancer models (Table 4). Although small sample numbers and the imaging considerations of the technique (Table 1) are potential limitations of these studies, their findings indicate that targeted therapies can affect the MRI-based vessel-calibre estimate in four ways.

First, the MRI data might provide evidence of a collective reduction in dilated tumour macrovessel and microvessel calibres suggesting an exhaustive response to therapy across all tumour vessel types. Such an effect was observed with a range of targeted therapies (Table 4), and—according to the VSI estimates (Box 1)—indicates reductions of a similar scale in macrovessel and microvessel blood volumes and calibres.[118,137–140] However, whereas reductions of macrovessel and microvessel calibres will result in a left-ward shift in the corresponding VSI distribution histogram (that is, towards smaller average vessel

diameters),[1,27,141,142] equally scaled reductions of macrovessel and microvessel calibres will result in no apparent change in the MRI-based relative mean vessel diameter estimate (mVD; Box 1)—that is, equal reductions of nominator and denominator.

Second, the MRI data might indicate a larger relative decrease in macrovessel blood volume and calibres compared with the decreases in microvessel parameters, indicating effective targeting of larger (radius >10 μm), abnormal tumour vessels.[87,119,143] This pattern will result in decreases in both the VSI and the mVD estimates.

Third, a larger relative decrease in microvessel blood volume and calibres compared with the change in these measurements of macrovessels might be suggested on the basis of the MRI data obtained.[120,144–147] This therapeutic response indicates selective targeting of small tumour vessels (radius <10 μm) compared with an apparent resistance of larger tumour vessels.[144,148–150] It is critically important to note that, according to the equation used to determine the mVD estimate (Box 1), a larger reduction in microvessel blood volume and calibres might in fact result in an apparent increase in the MRI-based average VSI estimate (Table 4), which is not to be mistaken for a true increase in individual vessel calibres.[6,99,120,148,151]

Fourth, the MRI data might show no apparent change in macrovessel and microvessel blood volume and calibres, indicating no effect of therapy or, alternatively, no effect at the specific dose used.[144,152–156]

Collectively, responses of tumour-vessel calibres after targeted treatment convey a complex picture dependent on not only tumour type and location,[21] and the therapeutic agent and dose used,[28] but also a dependence on the imaging parameters reported (microvessel calibres, macrovessel calibres or average VSI) as well as the timing of evaluation. Of note, no studies on antiangiogenic and antivascular therapies (Table 4) observe an apparent and transient increase in both microvessel and macrovessel vessel calibres.

Emerging data from trials in glioblastoma

The organizers of clinical trials seem undeterred by the challenges of conventional MRI, with close to 30 reported NIH-funded clinical imaging trials on bevacizumab in patients with glioblastomas alone—of which 10 are recruiting at the time of writing.[157] However, the lack of data derived from more-advanced imaging techniques is striking. To the best of our knowledge, Massachusetts General Hospital is the only institution that has reported on vessel-calibre MRI data obtained during antiangiogenic therapy in clinical studies (Table 3). In two phase II clinical trials of cediranib that enrolled 30 patients with recurrent glioblastomas,[158] and 40 patients with newly diagnosed glioblastomas,[159] our data demonstrated substantial reductions in abnormal macrovessel and microvessel calibres within tumours as early as 1 day after administration of this VEGFR inhibitor (Figure 3).[99,130,132] In the patients with newly diagnosed glioblastomas who responded to therapy, the reduction in tumour-vessel calibres was sustained throughout the 6-week period of cediranib treatment combined with temozolomide chemotherapy (75 mg/m^2) and radiotherapy (2 Gy per day).[132] Furthermore, reduced tumour permeability and increased tumour perfusion were seen in up to half of the patients included in these studies.[99,130,132]

These findings are in line with the vascular normalization hypothesis,[26,160] and were also reflected in increased overall survival.[132] However, after the 6-week period of antiangiogenic and adjuvant therapy, vessel normalization was reversed and relapse of vasogenic oedema was observed in most patients,[132] suggesting an end to the vascular normalization window. In a contemporary control study[161] in patients with newly diagnosed glioblastomas undergoing an identical MRI and chemoradiotherapy regimen, but without cediranib, reduced tumour-vessel calibres were only observed in one out of 14 patients (Supplementary Figure 2).[132]

These promising findings at our institution are in contrast to randomized phase III trials of cediranib in recurrent glioblastomas[162] and also trials of bevacizumab in newly diagnosed glioblastoma multiforme (AVAglio and RTOG 0825 trials[163,164]) that failed to show an overall survival benefit. On the basis of radiological response alone (according to a modified version of the MacDonald criteria) or in combination with improved neurological status, progression-free survival was prolonged after bevacizumab and chemoradiation (temozolomide) therapy in the AVAglio study, but not the RTOG 0825 study.[165] These disappointing effects of antiangiogenic therapy on survival indicate that the use of some targeted therapies is probably not favourable or ideal in unselected groups of patients with cancer and, in light of the findings from Massachusetts General Hospital, also suggests that imaging parameters from conventional MRI are inadequate biomarkers of response.

Suggestions for vessel-calibre MRI in trials

A number of key elements determine the success of a cancer-imaging clinical trial, including selection of an appropriate set of biomarkers for monitoring response to the therapy being studied, optimal imaging time points, and the use of a well-designed image acquisition protocol and correct methods of data analysis. Although advanced MRI is not part of the RECIST criteria,[42] the NCI Cancer Imaging Program does provide a set of guidelines for the application of advanced imaging modalities in clinical trials, including suggestions for DCE-MRI (for measuring tissue permeability).[166] We support these efforts to provide guidance to researchers, and complement these consensus guidelines with our suggestions for use of vessel-calibre MRI in the initial phases of trial design for studies of antiangiogenic and vascular-targeting agents (Box 2).

In short, the design of imaging trials is critically dependent on at least one baseline scan as close as possible to initiation of therapy, which should be followed by a second scan within the first days of therapy for assessment of early therapeutic response.[29] For studies of targeted therapies, repeated weekly or monthly follow-up imaging assessment is ideal—although counterbalanced by patient burden and costs—to observe the responses and plateaus in the various advanced-MRI parameters used, and to identify the end of the vascular normalization period (Figure 4).[8] Because of the apparent sensitivity of the technique to changes in vascularization, vessel-calibre MRI seems to have the potential to inform personalized therapy and to enable the optimal window of vascular normalization and potentially, therefore, drug administration to be determined in individual patients.

To achieve a sufficiently large patient population over a relatively short period of time (typically 1–3 years), presently, most clinical trials are multi-institutional studies. As

discussed by others, and although logistically challenging, a multicentre study design is essentially the only way of assessing the real physical process of therapeutic intervention independent of institutional variations.[64,121] With some exceptions,[167,168] vessel-calibre MRI—similar to most advanced imaging methods—suffers from lack of multicentre validation when applied alone in a research setting, or as part of a clinical trial. With careful planning,[121] vessel-calibre MRI is no more difficult to perform during a clinical trial than conventional contrast-enhanced MRI. Before the trial commences, multicentre variability in scanner performance and post-processing routines can be reduced by performing development studies in healthy volunteers or standardized phantom testing.[121] An MRI phantom test usually involves imaging of a magnetic-resonance-compatible polycarbonate plastic object with an array of small spheres or compartments that are filled with substances of different magnetic properties and with known scanning positions for calibration. The Alzheimer's Disease Neuroimaging Initiative (ADNI) phantom programme[169] is dedicated to this purpose, and has the added advantage of a centralized imaging-standard review process, which can reduce errors that contribute to quantitative imprecision. Indeed, this collaborative agreement was shown to identify MRI system failures that, if not corrected for, might have contributed to up to 25% imprecision in quantitative measures across institutions. Most importantly, the ADNI demonstrates that multicentre imaging standardization is achievable. For vessel-calibre MRI in particular, sufficient image quality with high signal-to-noise should be established early in the trial development processes in a small pilot study, before deciding on a standardized imaging protocol that should be used across multiple centres. Protocols should also capitalize on existing scanner-based and postprocessing software solutions to minimize the effects of imperfect patient positioning in the scanner, stochastic or free-breathing movements, as well as extravasation of gadolinium-based contrast agents (Supplementary Methods).[12,134,170]

Future directions

The most-pressing issue for imaging-response criteria for targeted therapies is the need for the introduction and validation of advanced imaging beyond the current RECIST and RANO criteria.[11,42,171] Future updated response criteria should include volumetric measurements, dynamic imaging and molecular imaging. The goals of these efforts are: firstly, smaller, cheaper, and selectively targeted patient populations for clinical trials; secondly, earlier and more-focused response assessments; and, thirdly, faster regulatory approvals of therapies than is currently possible for antiangiogenic and antivascular therapies. We believe that MRI-based measures of vessel calibres in solid tumours complement traditional imaging modalities and should play a part in any updated response criteria for antivascular and antiangiogenic therapies.

Composite biomarkers

Although efforts have been made to automate the vessel-calibre analysis protocol,[99] MRI biomarkers of such high complexity usually have the drawback of a laborious acquisition process compared with simpler response measures, such as tumour size. However, in comparison to traditional DSC-MRI-based estimations of blood volume, vessel-calibre MRI is no more difficult to perform and, because of its unique identification of microvessel and

macrovessel calibre, might help in bringing MRI one step closer to enabling personalized diagnoses for specific tumour subtypes and, thereby, facilitate the development of tailored therapeutic regimens. In conjunction with traditional MRI-based measures of tumour size and tumour-vessel permeability,[9] of which the latter has revealed consistent reductions of the permeability surface area product K^{trans} following antiangiogenic therapy,[9,13,15,17,59,172] vessel-calibre MRI might have utility as a companion indicator for tumour response to targeted nanoparticle-based EPR therapies in the future.[35,37] For example, angiotensin inhibitors, such as losartan, are known to effectively increase the diameters of blood vessels in models of matrix-rich breast tumours,[38] thus, vessel-calibre MRI could have value in assessing responses and guiding the use of such agents. However, for such composite biomarkers to have a role in clinical trials, they need to be validated in large, multicentre studies to overcome the 'curse of dimensionality', which is the concept that multiple input parameters require large amounts of data to support physiologically and statistically sound conclusions.[173]

Next-generation vessel architectural imaging

Vessel architectural imaging (VAI), which exploits a temporal shift in the macrovessel MRI signal compared with the microvessel signal (Supplementary Methods),[84,99,128] has been introduced as a new concept in vessel-calibre MRI assessment of cancer therapy.[99] This effect was first observed by Kiselev *et al.*[84] in 2005 and was attributed to the high sensitivity of the macrovessel MRI signal for deoxygenated capillary and venous blood volume; thus, the temporal shift might reveal information on the vessel types present (arteries, capillaries, or veins), as well as the relative difference in radii and oxygen saturation levels between these vessel types.[93,95,99,145] The highly intriguing link between this effect and oxygen saturation is in line with the BOLD effect,[174] as well as numerical modelling by Jespersen *et al.*[175] showing that heterogeneous perfusion from torturous microvessels and capillaries, resulting in varying contrast-agent arrival times and mean transit times, influences the maximum oxygen extraction fraction and the metabolic rate of oxygen use in tissues. In our imaging studies in trials of antiangiogenic therapy with cediranib, VAI revealed that overall survival duration was increased in 30–50% of patients with glioblastoma who had an observed reduction in abnormal tumour vessels, improved tumour perfusion, and normalization of the arteries-to-capillaries-to-veins branching hierarchy and oxygen saturation levels.[99,132] We are currently exploring the use of VAI in other tumours types and organs, including brain metastases, and breast and kidney tumours (Supplementary Figure 3). Importantly, an apparent wealth of information beyond a simple measure of the average vessel calibre can be obtained using VAI, such as tumour vascular structure and physiology.

Conclusions

The identification and interpretation of valid prognostic and predictive biomarkers for cancer diagnosis and assessment of therapeutic response is a major challenge in the field of oncology. Because of its high sensitivity to tumour physiology and vascular structure, vessel calibre is a possible biomarker for MRI-based *in vivo* cancer imaging, with the potential to provide new information and an increased understanding of the complex nature of tumour vascularity. With increased availability and awareness of the technique, combined with

optimization of imaging and scheduling protocols, we postulate that vessel-calibre MRI can have a direct effect on the efficacy of future antivascular and antiangiogenic clinical trials in patients with cancer.

Supplementary Material

Refer to Web version on PubMed Central for supplementary material.

Acknowledgements

The authors thank J. Martin (Department of Chemical Engineering, Massachusetts Institute of Technology and the Edwin L. Steele Laboratory of Tumor Biology, Massachusetts General Hospital) and T. Stylianopoulos (Department of Mechanical and Manufacturing Engineering, University of Cyprus) for help with this manuscript. The authors apologize to the authors whose work we could not cite owing to limits on the number of references that we were able to include. The authors acknowledge funding support from the National Cancer Institute, NIH, US Department of Human and Health Services (grants NCT00254943 to K.E.E., T32-CA009502 to C.T.F., NCT00756106 to E.R.G., NCT00662506 to T.T.B., S10 RR021110-01A1 to B.R.R., NCT00254943 to A.G.S. and P01CA80124 to R.K.J.), and the South-Eastern Norway Regional Health Authority (grant 2013069 to K.E.E.). In addition, R.J.H.B. acknowledges funding from the Sigrid Juselius Foundation, the Instrumentarium Research Foundation, the Academy of Finland, the Paulo Foundation and the Finnish Medical Foundation.

K.E.E. has intellectual property rights with NordicNeuroLab. T.T.B. is a consultant and/or is an advisory board member for Advance Medical, Agenus, Champions Biotechnology, Kirin Pharmaceuticals, Merck & Co. Inc., Novartis, Proximagen and Roche, and has received research funding from AstraZeneca, Millenium and Pfizer. B.R.R. is a consultant and an advisory board member for Siemens Medical. A.G.S. is the Chief Executive Officer for Siemens HealthCare USA. R.K.J. is on the Board of Directors of Xtuit; holds equity in Enlight, SynDevRx and Xtuit; and has received research funding from Dyax, Medimmune and Roche.

References

1. Jain RK. Molecular regulation of vessel maturation. Nat. Med. 2003; 9:685–693. [PubMed: 12778167]
2. Baluk P, Hashizume H, McDonald DM. Cellular abnormalities of blood vessels as targets in cancer. Curr. Opin. Genet. Dev. 2005; 15:102–111. [PubMed: 15661540]
3. Fukumura D, Duda DG, Munn LL, Jain RK. Tumor microvasculature and microenvironment: novel insights through intravital imaging in pre-clinical models. Microcirculation. 2010; 17:206–225. [PubMed: 20374484]
4. Stylianopoulos T, et al. Causes, consequences, and remedies for growth-induced solid stress in murine and human tumors. Proc. Natl Acad. Sci. USA. 2012; 109:15101–15108. [PubMed: 22932871]
5. Carmeliet P, Jain RK. Molecular mechanisms and clinical applications of angiogenesis. Nature. 2011; 473:298–307. [PubMed: 21593862]
6. Vakoc BJ, et al. Three-dimensional microscopy of the tumor microenvironment *in vivo* using optical frequency domain imaging. Nat. Med. 2009; 15:1219–1223. [PubMed: 19749772]
7. Nagy JA, Chang SH, Dvorak AM, Dvorak HF. Why are tumour blood vessels abnormal and why is it important to know? Br. J. Cancer. 2009; 100:865–869. [PubMed: 19240721]
8. Jain RK. Normalizing tumor microenvironment to treat cancer: bench to bedside to biomarkers. J. Clin. Oncol. 2013; 31:2205–2218. [PubMed: 23669226]
9. O'Connor JP, Jackson A, Parker GJ, Roberts C, Jayson GC. Dynamic contrast-enhanced MRI in clinical trials of antivascular therapies. Nat. Rev. Clin. Oncol. 2012; 9:167–177. [PubMed: 22330689]
10. Jain RK, et al. Biomarkers of response and resistance to antiangiogenic therapy. Nat. Rev. Clin. Oncol. 2009; 6:327–338. [PubMed: 19483739]
11. Wen PY, et al. Updated response assessment criteria for high-grade gliomas: response assessment in neuro-oncology working group. J. Clin. Oncol. 2010; 28:1963–1972. [PubMed: 20231676]

12. Lin NU, et al. Challenges relating to solid tumour brain metastases in clinical trials, part 1: patient population, response, and progression. A report from the RANO group. Lancet Oncol. 2013; 14:e396–e406. [PubMed: 23993384]
13. Leach MO, et al. The assessment of antiangiogenic and antivascular therapies in early-stage clinical trials using magnetic resonance imaging: issues and recommendations. Br. J. Cancer. 2005; 92:1599–1610. [PubMed: 15870830]
14. Michaelis LC, Ratain MJ. Measuring response in a post-RECIST world: from black and white to shades of grey. Nat. Rev. Cancer. 2006; 6:409–414. [PubMed: 16633367]
15. Morgan B. Opportunities and pitfalls of cancer imaging in clinical trials. Nat. Rev. Clin. Oncol. 2011; 8:517–527. [PubMed: 21522122]
16. Folkman J. Angiogenesis: an organizing principle for drug discovery? Nat. Rev. Drug Discov. 2007; 6:273–286. [PubMed: 17396134]
17. Ellis LM, Hicklin DJ. VEGF-targeted therapy: mechanisms of anti-tumour activity. Nat. Rev. Cancer. 2008; 8:579–591. [PubMed: 18596824]
18. Bergers G, Hanahan D. Modes of resistance to anti-angiogenic therapy. Nat. Rev. Cancer. 2008; 8:592–603. [PubMed: 18650835]
19. Ferrara N, Kerbel RS. Angiogenesis as a therapeutic target. Nature. 2005; 438:967–974. [PubMed: 16355214]
20. Padera TP, et al. Pathology: cancer cells compress intratumour vessels. Nature. 2004; 427:695. [PubMed: 14973470]
21. Jain RK. An indirect way to tame cancer. Sci. Am. 2014; 310:46–53. [PubMed: 24640331]
22. Wilson WR, Hay MP. Targeting hypoxia in cancer therapy. Nat. Rev. Cancer. 2011; 11:393–410. [PubMed: 21606941]
23. Dewhirst MW, Cao Y, Moeller B. Cycling hypoxia and free radicals regulate angiogenesis and radiotherapy response. Nat. Rev. Cancer. 2008; 8:425–437. [PubMed: 18500244]
24. Yeo SG, Kim JS, Cho MJ, Kim KH, Kim JS. Interstitial fluid pressure as a prognostic factor in cervical cancer following radiation therapy. Clin. Cancer Res. 2009; 15:6201–6207. [PubMed: 19773374]
25. Folkman J. Tumor angiogenesis: therapeutic implications. N. Engl. J. Med. 1971; 285:1182–1186. [PubMed: 4938153]
26. Jain RK. Normalizing tumor vasculature with anti-angiogenic therapy: a new paradigm for combination therapy. Nat. Med. 2001; 7:987–989. [PubMed: 11533692]
27. Winkler F, et al. Kinetics of vascular normalization by VEGFR2 blockade governs brain tumor response to radiation: role of oxygenation, angiopoietin-1, and matrix metalloproteinases. Cancer Cell. 2004; 6:553–563. [PubMed: 15607960]
28. Huang Y, Stylianopoulos T, Duda DG, Fukumura D, Jain RK. Benefits of vascular normalization are dose and time dependent—letter. Cancer Res. 2013; 73:7144–7146. [PubMed: 24265277]
29. Jain RK, Duda DG, Clark JW, Loeffler JS. Lessons from phase III clinical trials on anti-VEGF therapy for cancer. Nat. Clin. Pract. Oncol. 2006; 3:24–40. [PubMed: 16407877]
30. Van der Veldt AA, et al. Rapid decrease in delivery of chemotherapy to tumors after anti-VEGF therapy: implications for scheduling of anti-angiogenic drugs. Cancer Cell. 2012; 21:82–91. [PubMed: 22264790]
31. Chauhan VP, et al. Normalization of tumour blood vessels improves the delivery of nanomedicines in a size-dependent manner. Nat. Nanotechnol. 2012; 7:383–388. [PubMed: 22484912]
32. Arjaans M, et al. Bevacizumab-induced normalization of blood vessels in tumors hampers antibody uptake. Cancer Res. 2013; 73:3347–3355. [PubMed: 23580572]
33. Gerlowski LE, Jain RK. Microvascular permeability of normal and neoplastic tissues. Microvasc. Res. 1986; 31:288–305. [PubMed: 2423854]
34. Matsumura Y, Maeda H. A new concept for macromolecular therapeutics in cancer chemotherapy: mechanism of tumoritropic accumulation of proteins and the antitumor agent smancs. Cancer Res. 1986; 46:6387–6392. [PubMed: 2946403]

35. Prabhakar U, et al. Challenges and key considerations of the enhanced permeability and retention effect for nanomedicine drug delivery in oncology. Cancer Res. 2013; 73:2412–2417. [PubMed: 23423979]
36. Peer D, et al. Nanocarriers as an emerging platform for cancer therapy. Nat. Nanotechnol. 2007; 2:751–760. [PubMed: 18654426]
37. Chauhan VP, Jain RK. Strategies for advancing cancer nanomedicine. Nat. Mater. 2013; 12:958–962. [PubMed: 24150413]
38. Chauhan VP, et al. Angiotensin inhibition enhances drug delivery and potentiates chemotherapy by decompressing tumour blood vessels. Nat. Commun. 2013; 4:2516. [PubMed: 24084631]
39. Afaq A, Andreou A, Koh DM. Diffusion-weighted magnetic resonance imaging for tumour response assessment: why, when and how? Cancer Imaging. 2010; 10(A):S179–S188. [PubMed: 20880779]
40. Patterson DM, Padhani AR, Collins DJ. Technology insight: water diffusion MRI—a potential new biomarker of response to cancer therapy. Nat. Clin. Pract. Oncol. 2008; 5:220–233. [PubMed: 18301415]
41. van Osch MJ, Vonken EJ, Bakker CJ, Viergever MA. Correcting partial volume artifacts of the arterial input function in quantitative cerebral perfusion MRI. Magn. Reson. Med. 2001; 45:477–485. [PubMed: 11241707]
42. Therasse P, et al. New guidelines to evaluate the response to treatment in solid tumors. European Organization for Research and Treatment of Cancer, National Cancer Institute of the United States, National Cancer Institute of Canada. J. Natl Cancer Inst. 2000; 92:205–216. [PubMed: 10655437]
43. Macdonald DR, Cascino TL, Schold SC Jr, Cairncross JG. Response criteria for phase II studies of supratentorial malignant glioma. J. Clin. Oncol. 1990; 8:1277–1280. [PubMed: 2358840]
44. Gehan EA, Tefft MC. Will there be resistance to the RECIST (Response Evaluation Criteria in Solid Tumors)? J. Natl Cancer Inst. 2000; 92:179–181. [PubMed: 10655425]
45. Oxnard GR, et al. When progressive disease does not mean treatment failure: reconsidering the criteria for progression. J. Natl Cancer Inst. 2012; 104:1534–1541. [PubMed: 22927506]
46. Therasse P, Eisenhauer EA, Verweij J. RECIST revisited: a review of validation studies on tumour assessment. Eur. J. Cancer. 2006; 42:1031–1039. [PubMed: 16616487]
47. Twombly R. Criticism of tumor response criteria raises trial design questions. J. Natl Cancer Inst. 2006; 98:232–234. [PubMed: 16478740]
48. Nishino M, et al. Personalized tumor response assessment in the era of molecular medicine: cancer-specific and therapy-specific response criteria to complement pitfalls of RECIST. AJR Am. J. Roentgenol. 2012; 198:737–745. [PubMed: 22451534]
49. Llovet JM, et al. Design and endpoints of clinical trials in hepatocellular carcinoma. J. Natl Cancer Inst. 2008; 100:698–711. [PubMed: 18477802]
50. Rustin GJ, et al. Re: New guidelines to evaluate the response to treatment in solid tumors (ovarian cancer). J. Natl Cancer Inst. 2004; 96:487–488. [PubMed: 15026475]
51. Hoos A, et al. Improved endpoints for cancer immunotherapy trials. J. Natl Cancer Inst. 2010; 102:1388–1397. [PubMed: 20826737]
52. Scher HI, Morris MJ, Kelly WK, Schwartz LH, Heller G. Prostate cancer clinical trial end points: “RECIST” ing a step backwards. Clin. Cancer Res. 2005; 11:5223–5232. [PubMed: 16033840]
53. Faivre SJ, Bouattour M, Dreyer C, Raymond E. Sunitinib in hepatocellular carcinoma: redefining appropriate dosing, schedule, and activity end points. J. Clin. Oncol. 2009; 27:e248–e250. [PubMed: 19901099]
54. Sorensen AG, et al. Comparison of diameter and perimeter methods for tumor volume calculation. J. Clin. Oncol. 2001; 19:551–557. [PubMed: 11208850]
55. Goldberg SN, et al. Image-guided tumor ablation: standardization of terminology and reporting criteria. Radiology. 2005; 235:728–739. [PubMed: 15845798]
56. Reuter M, et al. Impact of MRI head placement on glioma response assessment. J. Neurooncol. 2014; 118:123–129. [PubMed: 24566765]

57. Brandsma D, Stalpers L, Taal W, Sminia P, van den Bent MJ. Clinical features, mechanisms, and management of pseudoprogression in malignant gliomas. Lancet Oncol. 2008; 9:453–461. [PubMed: 18452856]
58. Wong CS, van der Kogel AJ. Mechanisms of radiation injury to the central nervous system: implications for neuroprotection. Mol. Interv. 2004; 4:273–284. [PubMed: 15471910]
59. Waldman AD, et al. Quantitative imaging biomarkers in neuro-oncology. Nat. Rev. Clin. Oncol. 2009; 6:445–454. [PubMed: 19546864]
60. Gore JC, Manning HC, Quarles CC, Waddell KW, Yankeelov TE. Magnetic resonance in the era of molecular imaging of cancer. Magn. Reson. Imaging. 2011; 29:587–600. [PubMed: 21524870]
61. van den Bent MJ, Vogelbaum MA, Wen PY, Macdonald DR, Chang SM. End point assessment in gliomas: novel treatments limit usefulness of classical Macdonald's Criteria. J. Clin. Oncol. 2009; 27:2905–2908. [PubMed: 19451418]
62. Burrell JS, et al. MRI measurements of vessel calibre in tumour xenografts: comparison with vascular corrosion casting. Microvasc. Res. 2012; 84:323–329. [PubMed: 22921880]
63. Zaharchuk G. Theoretical basis of hemodynamic MR imaging techniques to measure cerebral blood volume, cerebral blood flow, and permeability. AJNR Am. J. Neuroradiol. 2007; 28:1850–1858. [PubMed: 17998415]
64. Ashton E, Riek J. Advanced MR techniques in multicenter clinical trials. J. Magn. Reson. Imaging. 2013; 37:761–769. [PubMed: 23526755]
65. Meier P, Zierler KL. On the theory of the indicator-dilution method for measurement of blood flow and volume. J. Appl. Physiol. 1954; 6:731–744. [PubMed: 13174454]
66. Neeman M, Dafni H. Structural, functional, and molecular MR imaging of the microvasculature. Annu. Rev. Biomed. Eng. 2003; 5:29–56. [PubMed: 14527310]
67. Fisel CR, et al. MR contrast due to microscopically heterogeneous magnetic susceptibility: numerical simulations and applications to cerebral physiology. Magn. Reson. Med. 1991; 17:336–347. [PubMed: 2062208]
68. Rosen BR, et al. Contrast agents and cerebral hemodynamics. Magn. Reson. Med. 1991; 19:285–292. [PubMed: 1881317]
69. Rosen BR, et al. Susceptibility contrast imaging of cerebral blood volume: human experience. Magn. Reson. Med. 1991; 22:293–299. [PubMed: 1812360]
70. Ogawa S, Lee TM, Kay AR, Tank DW. Brain magnetic resonance imaging with contrast dependent on blood oxygenation. Proc. Natl Acad. Sci. USA. 1990; 87:9868–9872. [PubMed: 2124706]
71. Bandettini PA, Wong EC, Jesmanowicz A, Hinks RS, Hyde JS. Spin-echo and gradient-echo EPI of human brain activation using BOLD contrast: a comparative study at 1.5 T. NMR Biomed. 1994; 7:12–20. [PubMed: 8068520]
72. Hoppel BE, et al. Measurement of regional blood oxygenation and cerebral hemodynamics. Magn. Reson. Med. 1993; 30:715–723. [PubMed: 8139453]
73. Kennan RP, Zhong J, Gore JC. Intravascular susceptibility contrast mechanisms in tissues. Magn. Reson. Med. 1994; 31:9–21. [PubMed: 8121277]
74. Weisskoff RM, Zuo CS, Boxerman JL, Rosen BR. Microscopic susceptibility variation and transverse relaxation: theory and experiment. Magn. Reson. Med. 1994; 31:601–610. [PubMed: 8057812]
75. Boxerman JL, Hamberg LM, Rosen BR, Weisskoff RM. MR contrast due to intravascular magnetic susceptibility perturbations. Magn. Reson. Med. 1995; 34:555–566. [PubMed: 8524024]
76. Kiselev VG, Posse S. Analytical model of susceptibility-induced MR signal dephasing: effect of diffusion in a microvascular network. Magn. Reson. Med. 1999; 41:499–509. [PubMed: 10204873]
77. Dennie J, et al. NMR imaging of changes in vascular morphology due to tumor angiogenesis. Magn. Reson. Med. 1998; 40:793–799. [PubMed: 9840821]
78. Donahue KM, et al. Utility of simultaneously acquired gradient-echo and spin-echo cerebral blood volume and morphology maps in brain tumor patients. Magn. Reson. Med. 2000; 43:845–853. [PubMed: 10861879]

79. Provenzale JM, Mukundan S, Barboriak DP. Diffusion-weighted and perfusion MR imaging for brain tumor characterization and assessment of treatment response. Radiology. 2006; 239:632–649. [PubMed: 16714455]
80. Covarrubias DJ, Rosen BR, Lev MH. Dynamic magnetic resonance perfusion imaging of brain tumors. Oncologist. 2004; 9:528–537. [PubMed: 15477637]
81. Oostendorp M, Post MJ, Backes WH. Vessel growth and function: depiction with contrast-enhanced MR imaging. Radiology. 2009; 251:317–335. [PubMed: 19401568]
82. Jensen JH, Chandra R. MR imaging of microvasculature. Magn. Reson. Med. 2000; 44:224–230. [PubMed: 10918321]
83. Tropres I, et al. Vessel size imaging. Magn. Reson. Med. 2001; 45:397–408. [PubMed: 11241696]
84. Kiselev VG, Strecker R, Ziyeh S, Speck O, Hennig J. Vessel size imaging in humans. Magn. Reson. Med. 2005; 53:553–563. [PubMed: 15723391]
85. Remmele S, et al. Concurrent MR blood volume and vessel size estimation in tumors by robust and simultaneous DeltaR2 and DeltaR2* quantification. Magn. Reson. Med. 2011; 66:144–153. [PubMed: 21305604]
86. Packard SD, et al. Functional response of tumor vasculature to $PaCO_2$: determination of total and microvascular blood volume by, MRI. Neoplasia. 2003; 5:330–338. [PubMed: 14511404]
87. Quarles CC, Schmainda KM. Assessment of the morphological and functional effects of the anti-angiogenic agent SU11657 on 9L gliosarcoma vasculature using dynamic susceptibility contrast MRI. Magn. Reson. Med. 2007; 57:680–687. [PubMed: 17390352]
88. Caravan P, Ellison JJ, McMurry TJ, Lauffer RB. Gadolinium(III) chelates as MRI contrast agents: structure, dynamics, and applications. Chem. Rev. 1999; 99:2293–2352. [PubMed: 11749483]
89. Schmiedeskamp H, et al. Simultaneous perfusion and permeability measurements using combined spin- and gradient-echo MRI. J. Cereb. Blood Flow Metab. 2013; 33:732–743. [PubMed: 23462570]
90. Kim SG, et al. Cerebral blood volume MRI with intravascular superparamagnetic iron oxide nanoparticles. NMR Biomed. 2013; 26:949–962. [PubMed: 23208650]
91. Farrar CT, et al. *In vivo* validation of MRI vessel caliber index measurement methods with intravital optical microscopy in a U87 mouse brain tumor model. Neuro Oncol. 2010; 12:341–350. [PubMed: 20308312]
92. Weinstein JS, et al. Superparamagnetic iron oxide nanoparticles: diagnostic magnetic resonance imaging and potential therapeutic applications in neurooncology and central nervous system inflammatory pathologies, a review. J. Cereb. Blood Flow Metab. 2010; 30:15–35. [PubMed: 19756021]
93. Christen T, et al. MR vascular fingerprinting: a new approach to compute cerebral blood volume, mean vessel radius, and oxygenation maps in the human brain. Neuroimage. 2014; 89:262–270. [PubMed: 24321559]
94. Jochimsen TH, Moller HE. Increasing specificity in functional magnetic resonance imaging by estimation of vessel size based on changes in blood oxygenation. Neuroimage. 2008; 40:228–236. [PubMed: 18248738]
95. Pannetier NA, Sohlin M, Christen T, Schad L, Schuff N. Numerical modeling of susceptibility-related MR signal dephasing with vessel size measurement: phantom validation at 3T. Magn. Reson. Med. http://dx.doi.org/10.1002/mrm.24968.
96. He X, Yablonskiy DA. Quantitative BOLD: mapping of human cerebral deoxygenated blood volume and oxygen extraction fraction: default state. Magn. Reson. Med. 2007; 57:115–126. [PubMed: 17191227]
97. Hsu YY, Yang WS, Lim KE, Liu HL. Vessel size imaging using dual contrast agent injections. J. Magn. Reson. Imaging. 2009; 30:1078–1084. [PubMed: 19856441]
98. Kiselev VG. Transverse relaxation effect of MRI contrast agents: a crucial issue for quantitative measurements of cerebral perfusion. J. Magn. Reson. Imaging. 2005; 22:693–696. [PubMed: 16261568]
99. Emblem KE, et al. Vessel architectural imaging identifies cancer patient responders to anti-angiogenic therapy. Nat. Med. 2013; 19:1178–1183. [PubMed: 23955713]

100. Kellner E, et al. Arterial input function measurements for bolus tracking perfusion imaging in the brain. Magn. Reson. Med. 2013; 69:771–780. [PubMed: 22610991]
101. Germuska MA, Meakin JA, Bulte DP. The influence of noise on BOLD-mediated vessel size imaging analysis methods. J. Cereb. Blood Flow Metab. 2013; 33:1857–1863. [PubMed: 23942365]
102. Lemasson B, et al. Assessment of multiparametric MRI in a human glioma model to monitor cytotoxic and anti-angiogenic drug effects. NMR Biomed. 2011; 24:473–482. [PubMed: 21674650]
103. Fredrickson J, et al. Clinical translation of VSI using ferumoxytol: feasibility in a phase I oncology clinical trial population [abstract]. Proc. Int. Soc. Mag. Reson. Med. (ISMRM) Annual Meeting. 2012:a1987.
104. Persigehl T, et al. Tumor blood volume determination by using susceptibility-corrected DeltaR2* multiecho MR. Radiology. 2010; 255:781–789. [PubMed: 20501715]
105. Wang Y-X. Superparamagnetic iron oxide based MRI contrast agents: current status of clinical application. Quant. Imaging Med. Surg. 2011; 1:35–40. [PubMed: 23256052]
106. Pannetier N, et al. Vessel size index measurements in a rat model of glioma: comparison of the dynamic (Gd) and steady-state (iron-oxide) susceptibility contrast MRI approaches. NMR Biomed. 2012; 25:218–226. [PubMed: 21751270]
107. Schmiedeskamp H, Straka M, Bammer R. Compensation of slice profile mismatch in combined spin- and gradient-echo echo-planar imaging pulse sequences. Magn. Reson. Med. 2012; 67:378–388. [PubMed: 21858858]
108. Paulson ES, Schmainda KM. Comparison of dynamic susceptibility-weighted contrast-enhanced MR methods: recommendations for measuring relative cerebral blood volume in brain tumors. Radiology. 2008; 249:601–613. [PubMed: 18780827]
109. Li SP, et al. Primary human breast adenocarcinoma: imaging and histologic correlates of intrinsic susceptibility-weighted MR imaging before and during chemotherapy. Radiology. 2010; 257:643–652. [PubMed: 20858850]
110. Benner T, Heiland S, Erb G, Forsting M, Sartor K. Accuracy of gamma-variate fits to concentration-time curves from dynamic susceptibility-contrast enhanced MRI: influence of time resolution, maximal signal drop and signal-to-noise. Magn. Reson. Imaging. 1997; 15:307–317. [PubMed: 9201678]
111. Li X, Tian J, Millard RK. Erroneous and inappropriate use of gamma fits to tracer-dilution curves in magnetic resonance imaging and nuclear medicine. Magn. Reson. Imaging. 2003; 21:1095–1096. [PubMed: 14684217]
112. Ito H, Kanno I, Ibaraki M, Hatazawa J, Miura S. Changes in human cerebral blood flow and cerebral blood volume during hypercapnia and hypocapnia measured by positron emission tomography. J. Cereb. Blood Flow Metab. 2003; 23:665–670. [PubMed: 12796714]
113. Ito H, Ibaraki M, Kanno I, Fukuda H, Miura S. Changes in the arterial fraction of human cerebral blood volume during hypercapnia and hypocapnia measured by positron emission tomography. J. Cereb. Blood Flow Metab. 2005; 25:852–857. [PubMed: 15716851]
114. Pathak AP, Ward BD, Schmainda KM. A novel technique for modeling susceptibility-based contrast mechanisms for arbitrary microvascular geometries: the finite perturber method. Neuroimage. 2008; 40:1130–1143. [PubMed: 18308587]
115. Tropres I, Lamalle L, Farion R, Segebarth C, Remy C. Vessel size imaging using low intravascular contrast agent concentrations. MAGMA. 2004; 17:313–316. [PubMed: 15580376]
116. Valable S, et al. Assessment of blood volume, vessel size, and the expression of angiogenic factors in two rat glioma models: a longitudinal *in vivo* and *ex vivo* study. NMR Biomed. 2008; 21:1043–1056. [PubMed: 18615861]
117. Kim E, et al. Assessing breast cancer angiogenesis *in vivo*: which susceptibility contrast MRI biomarkers are relevant? Magn. Reson. Med. 2013; 70:1106–1116. [PubMed: 23225578]
118. Persigehl T, et al. Vessel size imaging (VSI) by robust magnetic resonance (MR) relaxometry: MR-VSI of solid tumors in correlation with immunohistology and intravital microscopy. Mol. Imaging. 2013; 12:1–11. [PubMed: 23962676]

119. Ungersma SE, et al. Vessel imaging with viable tumor analysis for quantification of tumor angiogenesis. Magn. Reson. Med. 2010; 63:1637–1647. [PubMed: 20512867]
120. Bauerle T, Merz M, Komljenovic D, Zwick S, Semmler W. Drug-induced vessel remodeling in bone metastases as assessed by dynamic contrast enhanced magnetic resonance imaging and vessel size imaging: a longitudinal *in vivo* study. Clin. Cancer Res. 2010; 16:3215–3225. [PubMed: 20530698]
121. Tofts PS, Collins DJ. Multicentre imaging measurements for oncology and in the brain. Br. J. Radiol. 2011; 84(2):S213–S226. [PubMed: 22433831]
122. Larsen OA, Lassen NA. Cerebral hematocrit in normal man. J. Appl. Physiol. 1964; 19:571–574. [PubMed: 14195563]
123. Ostergaard L, Weisskoff RM, Chesler DA, Gyldensted C, Rosen BR. High resolution measurement of cerebral blood flow using intravascular tracer bolus passages. Part I: mathematical approach and statistical analysis. Magn. Reson. Med. 1996; 36:715–725. [PubMed: 8916022]
124. Schmainda KM, et al. Characterization of a first-pass gradient-echo spin-echo method to predict brain tumor grade and angiogenesis. AJNR Am. J. Neuroradiol. 2004; 25:1524–1532. [PubMed: 15502131]
125. Lamalle L, et al. VSI and BV MRI of human brain tumours [abstract]. Proc. 11th Annu. Meeting Int. Soc. Mag. Reson. Med. 2003:a1271.
126. Kiselev VG, et al. quantitative vessel size imaging in humans [abstract]. Proc. 11th Annu. Meeting Int. Soc. Mag. Reson. Med. 2003:a2192.
127. Breyer T, et al. Clinical evaluation of vessel size imaging in 31 cases of human glial brain tumor [abstract]. Proc. 15th Annu. Meeting Int. Soc. Mag. Reson. Med. 2007:a836.
128. Xu C, Kiselev VG, Moller HE, Fiebach JB. Dynamic hysteresis between gradient echo and spin echo attenuations in dynamic susceptibility contrast imaging. Magn. Reson. Med. 2013; 69:981–991. [PubMed: 22611004]
129. Pectasides M, et al. Evaluation of vessel size heterogeneity in brain tumors with dynamic contrast-enhanced dual echo perfusion weighted imaging [abstract]. Proc. 16th Annu. Meeting Int. Soc. Mag. Reson. Med. 2004:a152.
130. Batchelor TT, et al. AZD2171, a pan-VEGF receptor tyrosine kinase inhibitor, normalizes tumor vasculature and alleviates edema in glioblastoma patients. Cancer Cell. 2007; 11:83–95. [PubMed: 17222792]
131. Sorensen AG, et al. A “vascular normalization index” as potential mechanistic biomarker to predict survival after a single dose of cediranib in recurrent glioblastoma patients. Cancer Res. 2009; 69:5296–5300. [PubMed: 19549889]
132. Batchelor TT, et al. Improved tumor oxygenation and survival in glioblastoma patients who show increased blood perfusion after cediranib and chemoradiation. Proc. Natl Acad. Sci. USA. 2013; 110:19059–19064. [PubMed: 24190997]
133. Polaskova P, et al. Repeatability of MR-based vessel caliber estimates in brain tumor imaging [abstract]. Proc. Am. Soc. Neuroradiol. Annu. Meeting. 2013:O-404.
134. Lüdemann L, et al. Simultaneous quantification of perfusion and permeability in the prostate using dynamic contrast-enhanced magnetic resonance imaging with an inversion-prepared dual-contrast sequence. Ann. Biomed. Eng. 2009; 37:749–762. [PubMed: 19169821]
135. Jin N, et al. GESFIDE-PROPELLER approach for simultaneous R2 and R2* measurements in the abdomen. Magn. Reson. Imaging. 2013; 31:1760–1765. [PubMed: 24041478]
136. Yang X, et al. Evaluation of renal oxygenation in rat by using R2’ at 3-T magnetic resonance: initial observation. Acad. Radiol. 2008; 15:912–918. [PubMed: 18572128]
137. Ferretti S, et al. Patupilone induced vascular disruption in orthotopic rodent tumor models detected by magnetic resonance imaging and interstitial fluid pressure. Clin. Cancer Res. 2005; 11:7773–7784. [PubMed: 16278399]
138. Howe FA, McPhail LD, Griffiths JR, McIntyre DJ, Robinson SP. Vessel size index magnetic resonance imaging to monitor the effect of antivascular treatment in a rodent tumor model. Int. J. Radiat. Oncol. Biol. Phys. 2008; 71:1470–1476. [PubMed: 18538948]

139. Kording F, et al. Simultaneous assessment of vessel size index, relative blood volume, and vessel permeability in a mouse brain tumor model using a combined spin echo gradient echo echo-planar imaging sequence and viable tumor analysis. J. Magn. Reson. Imaging. http://dx.doi.org/10.1002/jmri.24513.
140. Nielsen T, et al. Combretastatin A-4 phosphate affects tumor vessel volume and size distribution as assessed using MRI-based vessel size imaging. Clin. Cancer Res. 2012; 18:6469–6477. [PubMed: 23071260]
141. Yuan F, et al. Vascular permeability and microcirculation of gliomas and mammary carcinomas transplanted in rat and mouse cranial windows. Cancer Res. 1994; 54:4564–4568. [PubMed: 8062241]
142. Kamoun WS, et al. Edema control by cediranib, a vascular endothelial growth factor receptor-targeted kinase inhibitor, prolongs survival despite persistent brain tumor growth in mice. J. Clin. Oncol. 2009; 27:2542–2552. [PubMed: 19332720]
143. Walker-Samuel S, et al. Non-invasive *in vivo* imaging of vessel calibre in orthotopic prostate tumour xenografts. Int. J. Cancer. 2012; 130:1284–1293. [PubMed: 21469141]
144. Zwick S, et al. Assessment of vascular remodeling under antiangiogenic therapy using DCE-MRI and vessel size imaging. J. Magn. Reson. Imaging. 2009; 29:1125–1133. [PubMed: 19388117]
145. Lemasson B, et al. Avastin alone or combined to Campto® reduces local blood oxygen saturation in an orthotopic human glioblastoma model (U87-MG) in nude rats [abstract]. Proc. 17th Annu. Meeting Int. Soc. Mag. Reson. Med. 2009:a1013.
146. Merz M, Komljenovic D, Zwick S, Semmler W, Bauerle T. Sorafenib tosylate and paclitaxel induce anti-angiogenic, anti-tumour and anti-resorptive effects in experimental breast cancer bone metastases. Eur. J. Cancer. 2011; 47:277–286. [PubMed: 20863686]
147. Zwick S, et al. Dynamic contrast-enhanced MRI and vessel size imaging sensitively indicate antiangiogenic therapy effects on tumor xenografts in mice [abstract]. Proc. 15th Annu. Meeting Int. Soc. Mag. Reson. Med. 2007:a564.
148. Farrar CT, et al. Sensitivity of MRI tumor biomarkers to VEGFR inhibitor therapy in an orthotopic mouse glioma model. PLoS ONE. 2011; 6:e17228. [PubMed: 21390238]
149. Woenne EC, et al. MMP inhibition blocks fibroblast-dependent skin cancer invasion, reduces vascularization and alters VEGF-A and PDGF-BB expression. Anticancer Res. 2010; 30:703–711. [PubMed: 20392987]
150. Palmowski M, et al. Vessel fractions in tumor xenografts depicted by flow- or contrast-sensitive three-dimensional high-frequency Doppler ultrasound respond differently to antiangiogenic treatment. Cancer Res. 2008; 68:7042–7049. [PubMed: 18757418]
151. Benjamin LE, Golijanin D, Itin A, Pode D, Keshet E. Selective ablation of immature blood vessels in established human tumors follows vascular endothelial growth factor withdrawal. J. Clin. Invest. 1999; 103:159–165. [PubMed: 9916127]
152. Remmele S, Senegas J, Persigehl T, Bremer C, Ring J. Simultaneous blood volume and vessel size imaging technique for localized therapy response detection [abstract]. Proc. 17th Annu. Meeting Int. Soc. Mag. Reson. Med. 2009:a4203.
153. Opstad KS, Howe FA. Vessel size index MRI to monitor the effects of vascular disruption by ASA404 (vadimezan, 5,6-dimethylxanthenone-4-acetic acid) in orthotopic gliomas [abstract]. Proc. 18th Annu. Meeting Int. Soc. Mag. Reson. Med. 2010:a4837.
154. Ullrich RT, et al. *In-vivo* visualization of tumor microvessel density and response to anti-angiogenic treatment by high resolution MRI in mice. PLoS ONE. 2011; 6:e19592. [PubMed: 21573168]
155. Boult JK, et al. False-negative MRI biomarkers of tumour response to targeted cancer therapeutics. Br J. Cancer. 2012; 106:1960–1966. [PubMed: 22596237]
156. Boult JK, Terkelsen J, Walker-Samuel S, Bradley DP, Robinson SP. A multi-parametric imaging investigation of the response of C6 glioma xenografts to MLN0518 (tandutinib) treatment. PLoS ONE. 2013; 8:e63024. [PubMed: 23638177]
157. US National Library of Medicine. ClinicalTrials.gov. 2014. [online], https://clinicaltrials.gov/ct2/results/refine?term=bevacizumab%C2%B1AND%C2%B1glioblastomas&fund=0

158. US National Library of Medicine. ClinicalTrials.gov. 2014. [online], https://clinicaltrials.gov/ct2/show/NCT00305656?term=NCT00254943&rank=1
159. US National Library of Medicine. ClinicalTrials.gov. 2014. [online], https://clinicaltrials.gov/ct2/show/NCT00662506?term=NCT00662506&rank=1
160. Jain RK. Normalization of tumor vasculature: an emerging concept in antiangiogenic therapy. Science. 2005; 307:58–62. [PubMed: 15637262]
161. US National Library of Medicine. ClinicalTrials.gov. 2014. [online], https://clinicaltrials.gov/ct2/show/NCT00756106?term=NCT00756106&rank=1
162. Batchelor TT, et al. Phase III randomized trial comparing the efficacy of cediranib as monotherapy, and in combination with lomustine, versus lomustine alone in patients with recurrent glioblastoma. J. Clin. Oncol. 2013; 31:3212–3218. [PubMed: 23940216]
163. Gilbert MR, et al. A randomized trial of bevacizumab for newly diagnosed glioblastoma. N. Engl. J. Med. 2014; 370:699–708. [PubMed: 24552317]
164. Chinot OL, et al. Bevacizumab plus radiotherapy-temozolomide for newly diagnosed glioblastoma. N. Engl. J. Med. 2014; 370:709–722. [PubMed: 24552318]
165. Weller M, Yung WK. Angiogenesis inhibition for glioblastoma at the edge: beyond AVAGlio and RTOG 0825. Neuro Oncol. 2013; 15:971. [PubMed: 23864129]
166. NCI Cancer Imaging Program. Imaging Guidelines for Clinical Trials. 2014. [online], http://imaging.cancer.gov/clinicaltrials/guidelines
167. Caseiras GB, et al. Relative cerebral blood volume measurements of low-grade gliomas predict patient outcome in a multi-institution setting. Eur. J. Radiol. 2010; 73:215–220. [PubMed: 19201123]
168. Ng CS, et al. Reproducibility of perfusion parameters in dynamic contrast-enhanced MRI of lung and liver tumors: effect on estimates of patient sample size in clinical trials and on individual patient responses. AJR Am. J. Roentgenol. 2010; 194:W134–W140. [PubMed: 20093564]
169. Gunter JL, et al. Measurement of MRI scanner performance with the ADNI phantom. Med. Phys. 2009; 36:2193–2205. [PubMed: 19610308]
170. Rosen BR, Belliveau JW, Vevea JM, Brady TJ. Perfusion imaging with NMR contrast agents. Magn. Reson. Med. 1990; 14:249–265. [PubMed: 2345506]
171. NCI Cancer Imaging Program. Imaging Response Criteria. 2014. [online], http://imaging.cancer.gov/clinicaltrials/imaging
172. Gaustad JV, Pozdniakova V, Hompland T, Simonsen TG, Rofstad EK. Magnetic resonance imaging identifies early effects of sunitinib treatment in human melanoma xenografts. J. Exp. Clin. Cancer Res. 2013; 32:93. [PubMed: 24245934]
173. Yang X, Knopp MV. Quantifying tumor vascular heterogeneity with dynamic contrast-enhanced magnetic resonance imaging: a review. J. Biomed. Biotechnol. 2011; 2011:732–848.
174. Christen T, Bolar DS, Zaharchuk G. Imaging brain oxygenation with MRI using blood oxygenation approaches: methods, validation, and clinical applications. AJNR Am. J. Neuroradiol. 2013; 34:1113–1123. [PubMed: 22859287]
175. Jespersen SN, Ostergaard L. The roles of cerebral blood flow, capillary transit time heterogeneity, and oxygen tension in brain oxygenation and metabolism. J. Cereb. Blood Flow Metab. 2012; 32:264–277. [PubMed: 22044867]
176. Sorensen AG, et al. Increased survival of glioblastoma patients who respond to antiangiogenic therapy with elevated blood perfusion. Cancer Res. 2012; 72:402–407. [PubMed: 22127927]
177. Badruddoja MA, et al. Antiangiogenic effects of dexamethasone in 9L gliosarcoma assessed by MRI cerebral blood volume maps. Neuro Oncol. 2003; 5:235–243. [PubMed: 14565159]
178. Tropres I, et al. *In vivo* assessment of tumoral angiogenesis. Magn. Reson. Med. 2004; 51:533–541. [PubMed: 15004795]
179. Beaumont M, et al. Characterization of tumor angiogenesis in rat brain using iron-based vessel size index MRI in combination with gadolinium-based dynamic contrast-enhanced MRI. J. Cereb. Blood Flow Metab. 2009; 29:1714–1726. [PubMed: 19584891]
180. Douma K, et al. Evaluation of magnetic resonance vessel size imaging by two-photon laser scanning microscopy. Magn. Reson. Med. 2010; 63:930–939. [PubMed: 20373394]

181. Lemasson B, et al. *In vivo* imaging of vessel diameter, size, and density: a comparative study between MRI and histology. Magn. Reson. Med. 2013; 69:18–26. [PubMed: 22431289]

182. Zhang Y, Jiang J, Zhang S, Xiong W, Zhu W. MR Vessel size imaging of brain tumors [abstract]. Proc. 98th Annu. Meeting Radiol. Soc. N. Am. 2012 LL-NRS-TU5A.

183. Viel T, et al. Non-invasive imaging of glioma vessel size and densities in correlation with tumour cell proliferation by small animal PET and MRI. Eur. J. Nucl. Med. Mol. Imaging. 2013; 40:1595–1606. [PubMed: 23754761]

184. Sampath D, et al. Multimodal microvascular imaging reveals that selective inhibition of class I PI3K is sufficient to induce an antivascular response. Neoplasia. 2013; 15:694–711. [PubMed: 23814482]

Key points

- Negative phase III trials suggest that administration of antiangiogenic therapies in unselected patient groups does not result in optimal outcomes, owing to diversity in cancer biology and natural history
- Antivascular and antiangiogenic therapies are not directly cytotoxic and, therefore, traditional assessment of MRI-based tumour volume change alone can no longer be considered an adequate biomarker of therapeutic response
- Intravascular paramagnetic contrast agents induce small and local magnetic field variations in tissue that scale with the blood vessel calibre (the cross-sectional width of the vessel)
- MRI is exquisitely sensitive to these magnetic field perturbations and, therefore, provides a means for *in vivo* assessment of tumour vessel calibre
- Depending on drug and dose administration, initial experiences with antivascular and antiangiogenic therapies and vessel-calibre MRI suggest that pruning of abnormal tumour vessels is often non-uniform
- Collectively, vessel-calibre MRI and emerging MRI-based assessments, such as vessel architectural imaging, can provide insights into vessel type and oxygenation status—creating new possibilities for clinical trial design and monitoring therapeutic response and outcomes

Box 1

Parameters used in vessel-calibre MRI

Mean vessel diameter (mVD)

mVD = $\Delta R_2^*/\Delta R_2$ ($\approx$ total blood volume MRI/microvessel blood volume MRI)

Mean vessel density (Q)‡

$Q = \Delta R_2/(\Delta R_2^*)^{2/3}$

For standard clinical contrast agent dosages, Q is independent of the contrast agent concentration.

Vessel size index (VSI)‡

$VSI = [k(V_f D)^{1/2}] \times ([\Delta R_2^*]/(\Delta R_2)^{3/2})$

‡Calculations of Q and VSI using a linear dependence on the quotient of macrovessel and microvessel volume fractions ($\Delta R_2^*/\Delta R_2$) show similar results to the preferred calculations using a proposed $^3/_2$ power dependence ($\Delta R_2^*/\Delta R_2^{3/2}$) attributed to the susceptibility effect (see Supplementary Methods online).[75,83,91] Abbreviations: ΔR_2, change over time in spin-echo relaxation rate; ΔR_2^*, change in gradient-echo relaxation rate; D, diffusion coefficient of water in tissue; k, proportionality constant; V_f, blood-volume fraction.

Box 2

Suggestions for vessel-calibre MRI in clinical trials of cancer

Study design

- Baseline imaging a short time (ideally 1 day) before initiation of therapy is essential, and an additional assessment a few days prior to this 'immediate' pretreatment measurement is recommended for calibration of data
- Changes in tumour vasculature following antivascular or antiangiogenic therapy are observed as early as day 1 of therapy and, therefore, imaging in the first days after initiation of therapy is critical
- Repeated imaging examinations using the same scanner with standardized imaging protocols are warranted within the first months of targeted therapy to detect the angiogenic switch, indicating the end of a vascular-normalization period
- For multicentre studies, enrollment of the full range of patients groups at all institutions is important

Imaging

- For gadolinium-based studies, a small amount of contrast agent (around 50% of the standard dose used) should be administered prior to the standard dose (pre-dose), in order to minimize conflicting contrast-agent extravasation effects
- Gadolinium-based assessment should also use a sufficiently high contrast-agent dose (≥1.0 mmol/kg) to compensate for the relative low signal-to-noise ratio achieved using microvessel (spin-echo) DSC-MRI
- Intravascular contrast agents (superparamagnetic iron oxide) are particularly useful for assessments of anatomical sites outside of the central nervous system; however, potential adverse effects of these agents, such as allergic reactions and back pain, are possible
- Diffusion-weighted MRI should be included in the imaging protocol to account for regional differences in diffusion, especially within the tumour
- Rapid echo planar imaging sequences can suffer from geometrical distortions; thus, image quality—both signal intensity images and relaxation rate maps—should be examined regularly during the study
- Variations in image geometry and imperfect patient positioning are major sources of error in longitudinal studies; all of the main instrument manufacturers provide atlas-based position registration systems that minimize variations between scans
- Efforts to reduce image variation should be made during the pilot phase by performing phantom imaging or assessment of healthy control individuals,

and image signal variations should be evaluated in homogenous tissue regions across institutions using matched controls

Image analysis and reporting

- DSC-MRI data are sensitive to motion and can be minimized by motion-correction algorithms or by orienting the patient and imaging slices so that the direction of motion is in-plane
- Correct for contrast-agent extravasation using mathematical correction algorithms
- High-resolution anatomical MRI and tumour regions-of-interest should be downscaled to vessel-calibre MRI resolution by automatic normalized mutual information co-registration procedures or similar algorithms
- Whole-tumour vessel distribution analysis is less sensitive to operator variations compared with 'hot-spot' region selection and yields higher reproducibility
- For multicentre studies, centralized tumour-region outlining and automatic analysis routines should be considered
- Tumour-vessel calibres during therapy should be reported relative to baseline values to reduce inter-patient variations and to adjust for global systemic vascular effects
- Reporting of patient-level macrovessel (ΔR_2*) and microvessel (ΔR_2) blood-volume data in a tabular form enables readers to understand the vascular response to therapy and to compare the published data with their own experimental data

Abbreviations: ΔR2, change in spin-echo relaxation rate; ΔR2*, change in gradient-echo relaxation rate; DSC-MRI, dynamic susceptibility-contrast MRI.

Review criteria

PubMed, MEDLINE and ISI Web of Knowledge databases were searched for full-text English-language articles published before 24 January 2014 using the following terms: “MRI AND vessel size” or “MRI AND vessel caliber”. The reference lists of the relevant articles identified were searched for additional papers. In addition, abstracts from ASCO, American Association for Cancer Research (AACR), Radiological Society of North America (RSNA), and International Society for Magnetic Resonance in Medicine (ISMRM) conferences were considered for inclusion if they provided relevant data that had not been published in full-text articles.

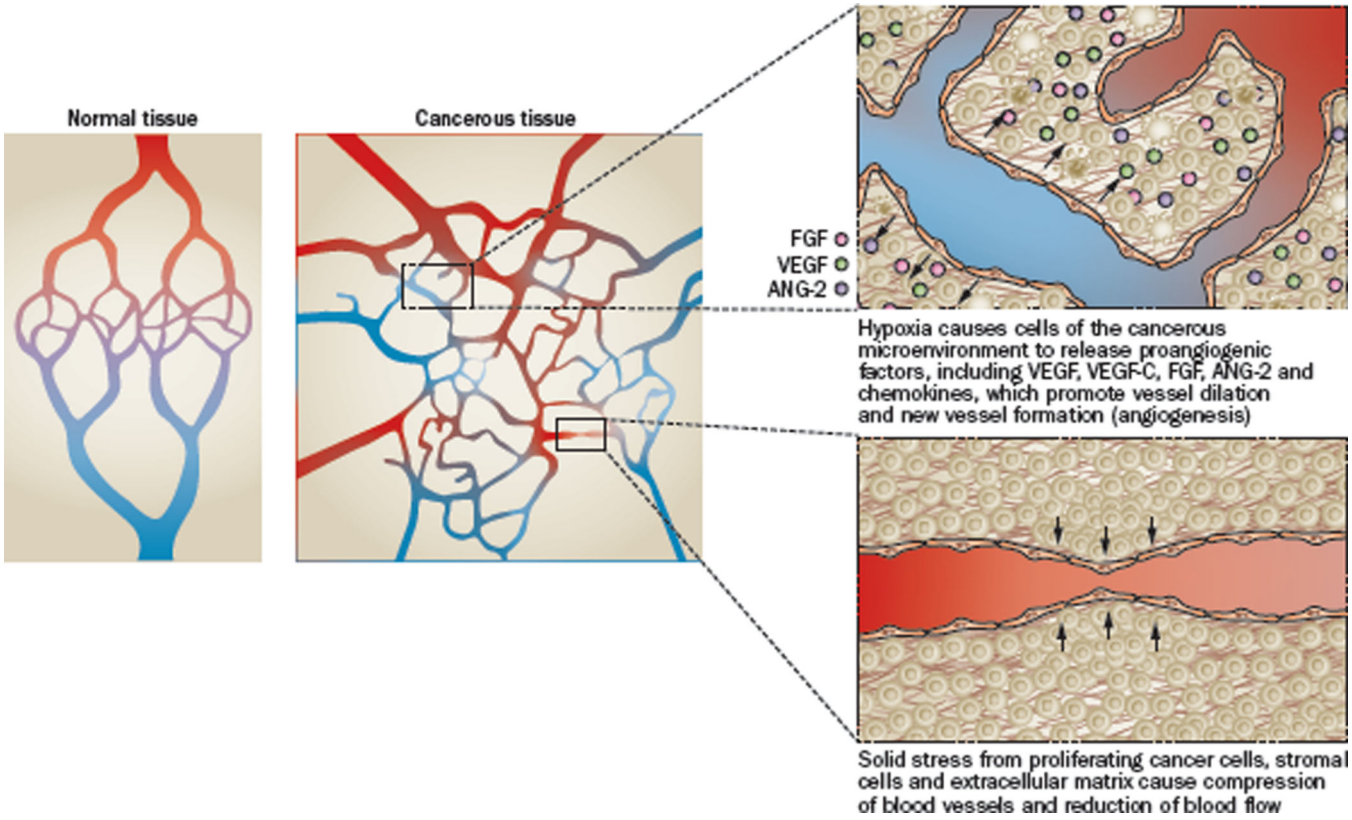

Figure 1.

Vessel calibres in solid cancers. Conceptual illustration showing key factors for vessel-calibre growth and remodelling within a tumour, including vessel dilatation after stimulation by proangiogenic factors such as VEGF, FGFs, ANG-2 and chemokines,[5] and compression of vessels as a result of solid stress induced by tumour growth.[4] In normal tissues, red vessels indicate oxygen-rich feeding arteries and arterioles, blue vessels are veins carrying deoxygenated blood and the intermediate regions indicate a transient capillary stage. In cancerous tissues, slow blood flow is indicated by reduced colour intensity. Abbreviations: ANG-2, angiopoietin-2; FGFs, fibroblast growth factors; VEGF, vascular endothelial growth factor.

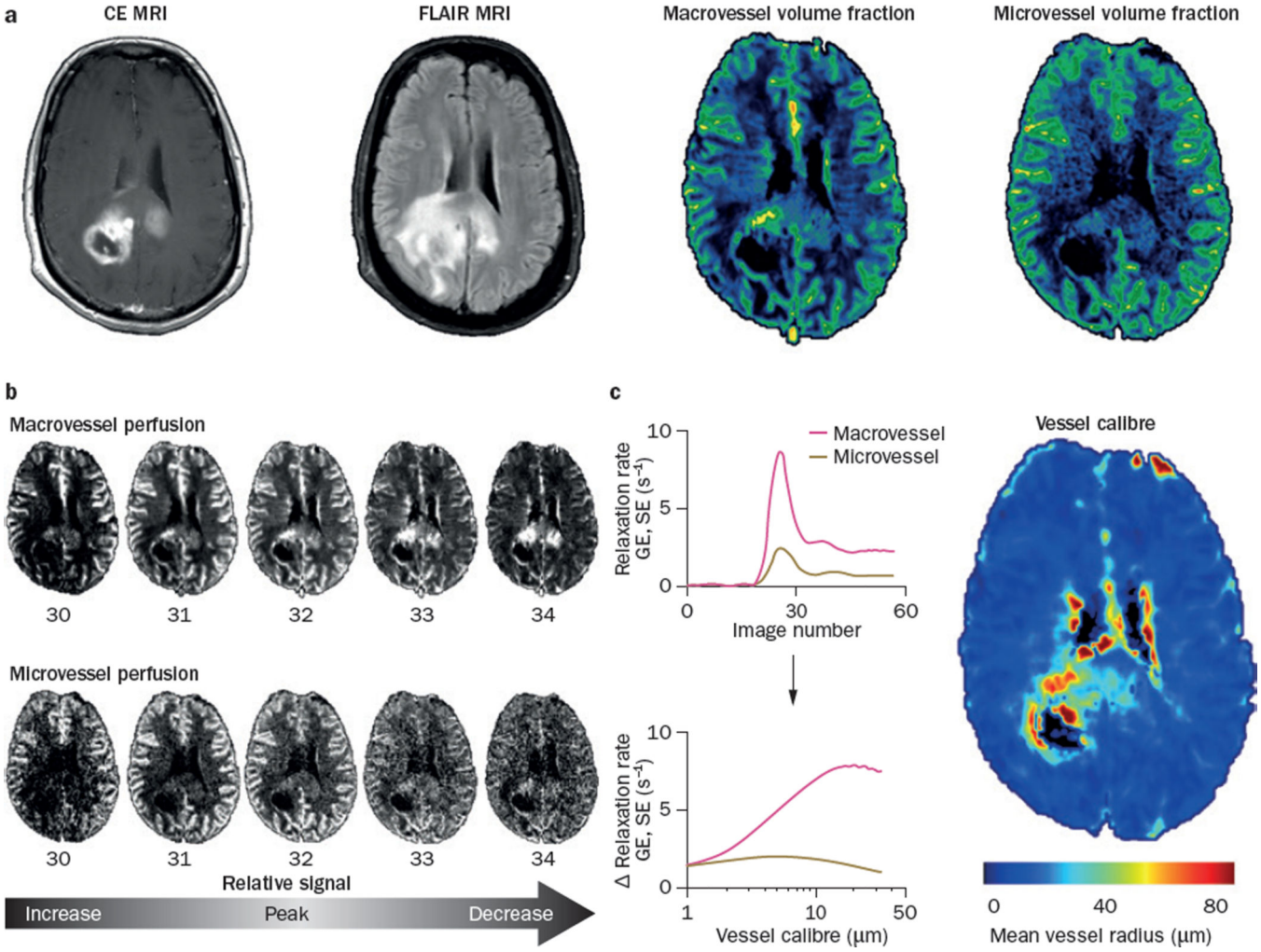

Figure 2.

Vessel-calibre MRI. **a** | Example anatomical CE T_1-weighted, FLAIR, macrovessel volume-fraction and microvessel volume-fraction images from MRI assessments of a patient with glioblastoma. Note the sensitivity to high blood-volume fractions in the macrovessel image (total blood volume) compared with the microvessel image. **b** | Macrovessel and microvessel DSC-MRI in the same patient with glioblastoma, with contrast agent passing through the tissue. Before estimation of perfusion and vessel-calibre MRI parameters, the macrovessel (GE) and microvessel (SE) blood-volume relaxation rate images shown here are computed according to the relative decrease in MRI signal intensity over the course of a sequence of GE MRI and SE MRI images, respectively (images 30–34 in this case), thereby adjusting for baseline intensity values and image sampling time (echo time). The so-called ‘first-pass effect’ denotes the initial and transient passage of a relatively tight bolus of the contrast agent following intravenous administration of the agent and is observed as a peak in the relative relaxation rate signal (peaks for normal tissue approximately at image 32). The contrast agent first-pass effect is particularly dominant in large vessels in the macrovessel images because of high contrast agent concentrations combined with high sensitivity to the magnetic susceptibility effect induced by the agent. After the initial first-pass contrast agent

passage, repeated passages of what remains of the circulating and increasingly dispersed contrast agent bolus can be appreciated as smaller and dissipating signal oscillations. **c** | Macrovessel and microvessel volume fractions are estimated from the area under the GE and SE first-pass curves (top left), respectively. The concept of vessel-calibre MRI stems from the relationship between increased macrovessel volume fractions for increasing vessel calibres, and microvessel volume fractions, which are selectively sensitive to small (radius <10 μm) vessel calibres (bottom left). Mean vessel density maps (Box 1) are thus derived from the quotient of macrovessel and microvessel volume fractions, whereas the vessel-calibre index also accounts for water diffusion and the absolute blood volume fraction. Abbreviations: CE, contrast-enhanced; DSC-MRI, dynamic susceptibility-contrast MRI; FLAIR, fluid-attenuated inversion recovery; GE, gradient-echo; SE, spin-echo.

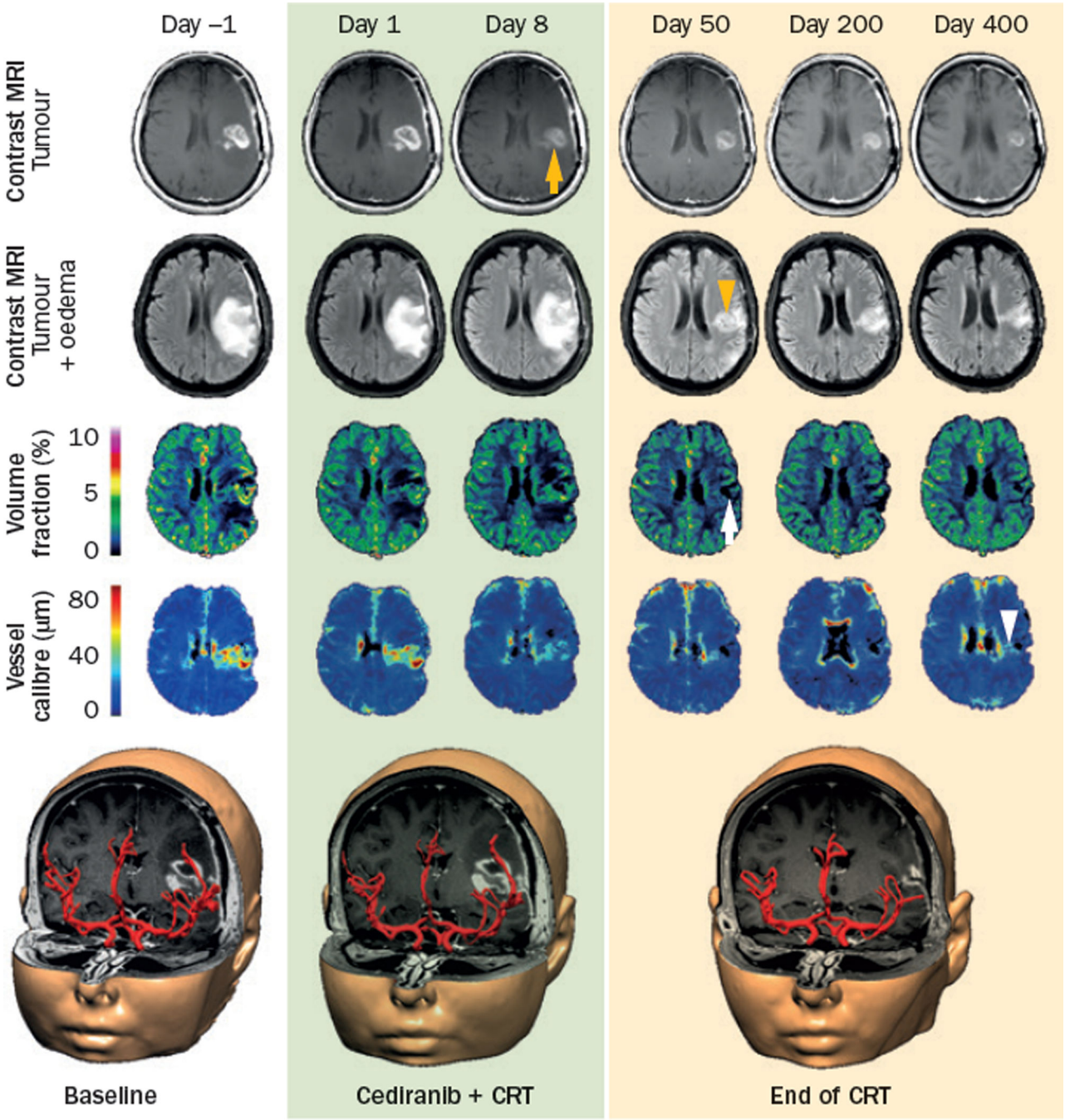

Figure 3.

Vessel-calibre MRI during antiangiogenic therapy. Selected MRI-derived images obtained over the course of a phase II trial of cediranib combined with CRT[159] in adult patients with newly diagnosed glioblastomas. From top to bottom: contrast-enhanced T_1-weighted MRI illustrating a permeable tumour vasculature; FLAIR MRI showing the tumour and vasogenic oedema; macrovessel blood-volume fractions; vessel-calibre maps; and volume renderings from 3D anatomical MRI with time-of-flight MRI angiography. Compared with pretreatment baseline images (day −1), cediranib therapy (days 1 and 8) decreased the signal

enhancement in the tumour, indicative of reduced permeability of the tumour vasculature, by day 8 (yellow arrow), and oedema was subsequently reduced (yellow arrowhead; day 50). Treatment effects of antiangiogenic and adjuvant combination therapy were also observed after the end of CRT (up to day 400); however, the cancer eventually relapsed and progressed, although this outcome is not clear using standard contrast and FLAIR MRI protocols. Volume fractions and vessel calibres show reductions that are related to the responses observed by conventional contrast-enhanced and FLAIR MRI following therapy (white arrow; day 50), but the vessel-calibre response also reveals unique properties of tissue that do not match the spatial distribution of the volume-fraction map. In contrast to the major vessels identified by standard MRI angiography (bottom panels), the vessel-calibre map depicts changes in the tumour microvasculature that are well below the image resolution achievable using the conventional approach; note the increased vessel calibres in the relapsed tumour region (white arrowhead; day 400), which is not easily appreciated on conventional MRI nor on the volume-fraction map. Abbreviations: CRT, chemoradiation therapy; FLAIR, fluid-attenuated inversion recovery.

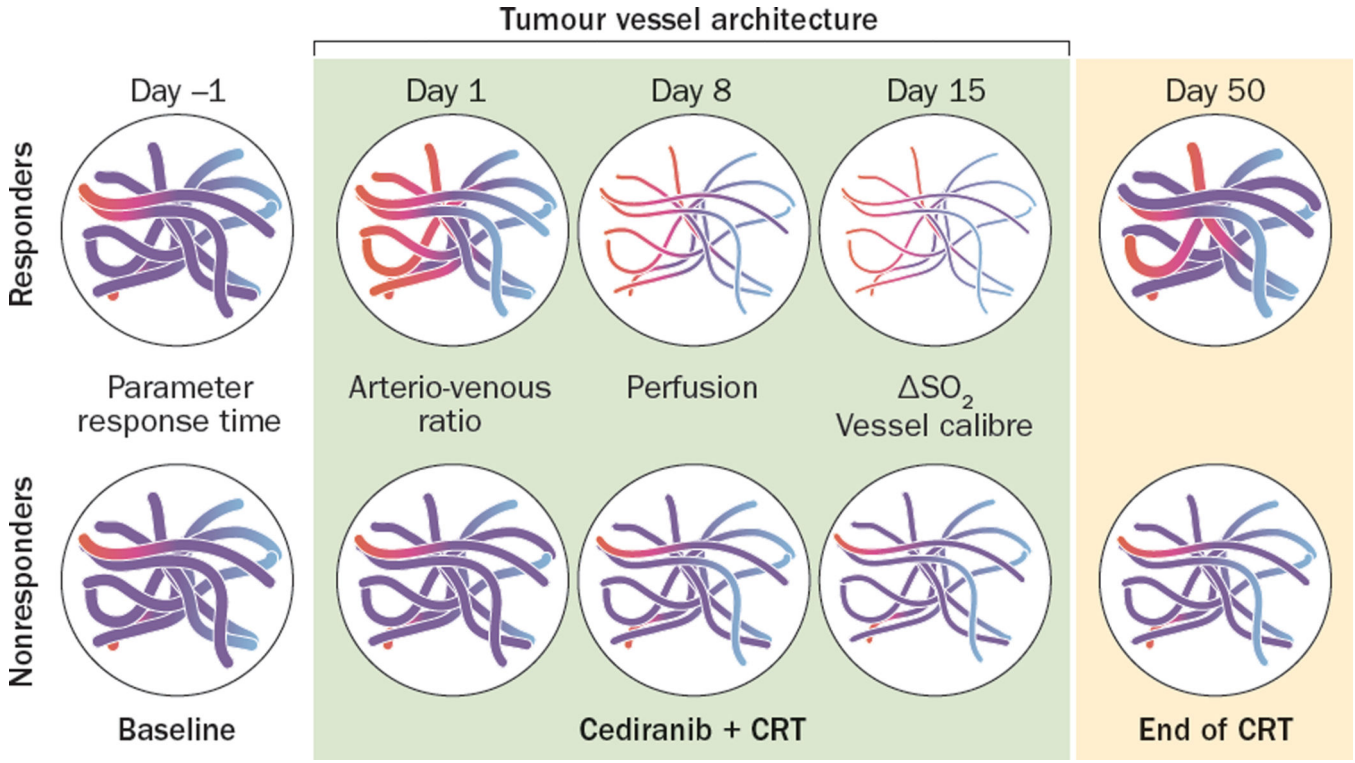

Figure 4.

Advanced MRI assessments might inform optimal dose scheduling. On the basis of our experience with cediranib,[99,130,132,176] the initial responses, plateaus and reversals in tumour response that are observed using advanced MRI parameters occur at different timepoints after initiation of therapy. In this example model of tumour-vessel architecture, showing a typical vascular-normalization response after cediranib treatment and CRT in patients with newly diagnosed glioblastomas,[132] the perfusion estimate (blood flow) peaks after approximately 1 week of therapy (day 8), whereas the maximum reduction in vessel calibres occurs 1 week later (day 15; note the reduced diameter of the example vessels). These effects are preceded by an early, substantial, and prolonged normalization of the abnormal arterio-venous ratio evident in the model of the baseline data (day 1; arteries/arteriole shown in red, with veins in blue), estimated using vessel architectural imaging. Consistent with the vessel-calibre response, the apparent change in abnormal ΔSO_2 levels reaches its minimum at two weeks (day 15; purple colour). After the end of CRT, all of these parameters reverse, thereby indicating an end to the vascular-normalization window. Furthermore, in patients who were deemed unresponsive to therapy, limited evidence of such responses was seen. Collectively, advanced MRI protocols might facilitate the design of improved early-phase trials by informing the optimization of the dosing regimen for antiangiogenic agents and could also potentially support a personalized-medicine approach by enabling therapy to be tailored to individual patients based on parameters indicative of biological and, in particular, vascular responses. In addition, early identification of patients who are unlikely to respond to therapy could help decision making regarding whether

therapy should be discontinued, particularly in patients who experience adverse events.
Abbreviations: ΔSO_2, relative oxygen saturation levels; CRT, chemoradiation therapy.

Table 1

Vessel-calibre MRI methodology

Imaging protocols	Contrast agent*	Target organs*	Computations	Imaging considerations‡
DSC GE/SE MRI	Gadolinium, SPIO	CNS, non-CNS	$\Delta R_2(t) = (1/TE)\ln(SI_t/SI_{t0})$ $\Delta R_2^* = (1/TE^*)\ln(SI_t^*/SI_{t0}^*)$	High temporal resolution Low spatial resolution Nonlinear MRI signal in bulk blood Gadolinium: extravasation correction required VSI overestimation compared with histological assessment
SSCE GE/SE MRI	SPIO, gadolinium, MION	Non-CNS, CNS	$\Delta R_2 = (1/TE)\ln(SI_{pre}/SI_{post})$ $\Delta R_2^* = (1/TE^*)\ln(SI_{pre}^*/SI_{post}^*)$ or $\Delta R_2^* = R_2^*{}_{post} - R_2^*{}_{pre}$	High spatial resolution Nonlinear MRI signal in bulk blood SPIO: high SNR owing to long half-life SPIO: not approved for clinical use VSI overestimation compared with histological assessments Contrast must remain intravascular or stable
BOLD MRI	Challenge with normoxic/carbogen gas or brain-activation stimuli	CNS	$\Delta R_2 = (1/TE)\ln(SI_{pre}/SI_{post})$ $\Delta R_2^* = (1/TE^*)\ln(SI_{pre}^*/SI_{post}^*)$ or $\Delta R_2^* = R_2^*{}_{post} - R_2^*{}_{pre}$	High temporal resolution Low geometric and flow-related distortions Low SNR Enables measurement of venous vessel calibres only Overestimation of mean vessel density in capillaries Underestimation of mean vessel density in bulk blood

*Listed in order of preference.

‡If clinical MRI field strengths (1.5T or preferably 3T) are used.

Abbreviations: ΔR_2, change in spin-echo relaxation rate; ΔR_2^*, change in gradient-echo relaxation rate; BOLD, blood-oxygen-level-dependent; CNS, central nervous system; DSC, dynamic susceptibility contrast; GE, gradient-echo; MION, monocrystalline iron oxide nanocompounds; $R_2^*{}_{post}$, gradient-echo relaxation rate image readout after contrast-injection; $R_2^*{}_{pre}$, gradient-echo relaxation rate image readout before contrast-injection; SE, spin-echo; SI_{post}, MRI signal intensity after contrast-injection; SI_{pre}, MRI signal intensity before contrast-injection; SI_t, signal intensity over time; SI_{t0}, signal intensity at baseline; SNR, signal-to-noise ratio; SPIO, super-paramagnetic iron oxide particles; SSCE, steady-state contrast-enhanced imaging prior to and after contrast injection; TE, image sampling time (echo time); VSI, weighted mean of vessel size index.

Table 2

Vessel-calibre MRI preclinical validation studies

Study	Tumour model	Model	Treatment administered	Validated method used for comparison	MRI-derived NmVD ± SD (number of samples)	NmVD ± SD derived using validated method (number of samples)
Dennie *et al.* (1998)[77]	C6 glioma	Rat	None	Histology	1.92 ± 0.24 (4)	1.89 ± 1.19 (3)
Badruddoja *et al.* (2003)[177]	9L gliosarcoma	Rat	Dexamethasone or vehicle	Histology	Dexamethasone: 1.91 ± 1.26 (17) Vehicle: 5.37 ± 3.56 (10)	Dexamethasone: 1.88 ± 0.28 (13) Vehicle: 2.97 ± 0.32 (7)
Packard *et al.* (2003)[86]	U87 glioma*	Rat	None	Histology	1.52 ± 0.63 (14)	1.63 ± 0.14 (6)
Tropres *et al.* (2004)[178]	C6 glioma	Rat	None	Histology	2.70 ± 0.65 (7)	1.87 ± 1.54 (7)
Valable *et al.* (2008)[116]	C6 glioma RG2 glioma	Rat	None	Histology	C6 glioma: 2.18 ± 0.50 (12) RG2 glioma: 1.79 ± 0.42 (12)	C6 glioma: 2.68 ± 0.61 (12) RG2 glioma 1.90 ± 0.39 (12)
Beaumont *et al.* (2009)[179]	C6 glioma RG2 glioma	Rat	None	Histology	C6 glioma: 2.82 ± 0.34 (14) RG2 glioma: 1.71 ± 0.17 (6)	C6 glioma: 1.59 ± 0.20 (6) RG2 glioma: 1.71 ± 0.15 (6)
Farrar *et al.* (2010)[91]	U87 glioma	Mouse	None	Histology Intravital microscopy	MRI (histology samples): 1.64 ± 0.10 (4) MRI (intravital microscopy samples): 1.39 ± 0.17 (7‡)	Histology: 1.67 ± 0.67 (4) Intravital microscopy: 1.37 ± 0.08 (5‡)
Douma *et al.* (2010)[180]	LS174T colorectal cancer§	Mouse	None	*Ex vivo* 3D laser scanning microscopy	2.88// (8‡)	1.95// (11‡)
Lemasson *et al.* (2011)[102]	U87 glioma	Rat	None, carmustine (BCNU), or sorafenib	Histology	No treatment: 1.20 ± 0.19 (4) BCNU: 1.20 ± 0.19 (4) Sorafenib: 1.55 ± 0.23 (4)	No treatment: 1.24 ± 0.15 (4) BCNU: 1.29 ± 0.16 (4) Sorafenib: 1.38 ± 0.17 (4)
Lemasson *et al.* (2013)[181]	C6 glioma RG2 glioma	Rat	None	Histology	C6 glioma: 1.62 ± 0.46 (15) RG2 glioma: 1.44 ± 0.48 (12)	C6 glioma: 1.69 ± 0.23 (15) RG2 glioma: 1.30 ± 0.30 (12)

*Average of baseline hypercarbia and hypocarbia groups.

‡Separate size-matched tumour samples used for MRI and validation assessments.

§Tumour core was analysed.

//SD not reported.

Abbreviations: BCNU, bischloroethylnitrosourea; NmVD, normalized mean vessel diameters (tumour-to-reference tissue ratio); SD, standard deviation.

Table 3

Clinical cancer studies including vessel-calibre MRI

Study	Cancer type	Number of patients (women/men)	Treatment administered	Findings
Donahue *et al.* (2000)[78]	Glioma* (*n* = 13) Lymphoma (*n* = 2)	15 adults (6/9)	NA	Vessel calibre was larger in the tumour than in healthy tissue, and increased with malignancy grade
Lamalle *et al.* (2003)[125]	Glioma*	9 patients‡	NA	Vessel calibre was larger in the tumour and lower in necrotic pars than in healthy tissue
Kiselev *et al.* (2003)[126]	Glioma* (*n* = 13) Meningioma (*n* = 4) Metastasis (*n* = 3)	20 patients‡	NA	Vessel calibre was larger in the tumour than in healthy tissue, and increased with malignancy grade
Schmainda *et al.* (2004)[124]	Glioma* (*n* = 72) Neurocytoma (*n* = 1)	73 adults (27/46)	NA	Vessel calibre was larger in the tumour than in healthy tissue, and increased with malignancy grade
Pectasides *et al.* (2004) [129]	Glioma*	9 patients‡	NA	Vessel calibre was more heterogeneous in the tumour than in adjacent tissue
Kiselev *et al.* (2005)[84]	Glioma* (*n* = 2) Meningioma (*n* = 2)	4 patients‡	NA	Vessel calibre was larger in the tumour than in healthy tissue, and increased with malignancy grade
Batchelor *et al.* (2007) [130]	Recurrent glioblastoma	16 adults[158] (9/7)	Cediranib (45 mg/kg per day)	Vessel calibre was markedly reduced at day 1 after treatment
Breyer *et al.* (2007)[127]	Glioma*	31 patients‡	NA	Vessel calibre was larger in the tumour than in healthy tissue, and increased with malignancy grade
Hsu *et al.* (2009)[97]	Glioma* (*n* = 5) Meningioma (*n* = 3)	8 adults (4/4)	NA	Vessel calibre was larger in the tumour than in healthy tissue, and increased with malignancy grade
Sorensen *et al.* (2009) [131]	Recurrent glioblastoma	30 adults[158] (13/17)	Cediranib (45 mg/kg per day)	Vessel calibre was markedly reduced at day 1 after treatment
Lüdemann *et al.* (2009)[134]	Prostate cancer	13 adults‡	NA	Vessel calibre was larger in the tumour than in healthy tissue
Remmele *et al.* (2011)[85]	Pleomorphic sarcoma	1 adult‡	NA	Repeated monitoring by vessel-calibre MRI shown to be feasible
Schmiedeskamp *et al.* (2012)[107]	Glioblastoma	1 patient‡	Radiotherapy (dose not reported)	Increased vessel calibres and vascular supply attributed to progressive disease, not pseudoprogression
Zhang *et al.* (2012)[182]	Glioma* (*n* = 14) Meningioma (*n* = 14)	28 adults (17/11)	NA	Vessel calibre was larger in the tumour than in healthy tissue, and increased with malignancy grade
Fredrickson *et al.* (2012)[103]	Colorectal metastasis	3 patients‡	NA	Mean vessel density estimation with SPIO agents

Study	Cancer type	Number of patients (women/men)	Treatment administered	Findings
				was feasible and well tolerated
Xu *et al.* (2013)[128]	Glioma* (*n* = 2) Meningioma (*n* = 2)	4 patients‡	NA	Vessel calibre was larger in the tumour than in healthy tissue
Emblem *et al.* (2013)[99]	Recurrent glioblastoma	30 adults[158] (13/17)	Cediranib (45 mg/kg per day)	Vessel calibre was markedly reduced at 1, 28 and 58 days after treatment
Batchelor *et al.* (2013) [132]	Newly diagnosed gliobastoma	40 adults[159] (13/27) 14 adults[161] (8/6)	Cediranib (30 mg/kg per day) and temozolomide (75 mg/m^2) and radiotherapy (2 Gy per day)	Vessel calibre was markedly reduced at days 1, 8, 15, 22, 29, 36 and 43 after treatment[159] Vessel calibre decreased in 1/14 patients treated with only temozolomide and radiotherapy[161]

*Several glioma subtypes included in the study.

‡Information on patient age and/or gender not reported.

Abbreviations: NA, not administered; SPIO, super-paramagnetic iron oxide particles.

Table 4

Preclinical antivascular and antiangiogenic studies that used vessel-calibre MRI

Treatment approach	Cancer model (number of animals)	Change in microvessel calibres	Change in macrovessel calibres	Time of response after therapy
Microtubule stabilization				
Patupilone; single 0.8 mg/kg dose	BN472 mammary carcinoma in rats (51)[137]	↓ (P <0.01)	↓ (P <0.01)	Day 6
RTK inhibition				
SU11657 (FLT3 inhibitor); 20 mg/kg or 40 mg/kg per day	9L gliosarcoma in rats (18)[87]	20 mg/kg: NC 40 mg/kg: ↓ (P <0.05)	20 mg/kg: ↓ (P <0.05) 40 mg/kg: ↓↓ (P <0.05)	Day 1–4 in both groups
Sunitinib (multitarget RTK inhibitor); 60 mg/kg per day	MDA-MB-435 melanoma in mice (10)[118]	↓ (P <0.05)	↓ (P <0.05)	Day 7
Sunitinib; 60 mg/kg per day	A431 SCC in mice (14)[144]	↓ (P <0.01)*	NC	Day 4
Sunitinib; 40 mg/kg every 3 days	HT1080 human breast fibrosarcoma in mice (NR)[152]	NC	NC	Days 4 and 7
Sunitinib (20 mg/kg per day) ± zoledronic acid (bisphosphonate; 40 mg/kg per week), or zoledronic acid alone	Bone metastases from MDA-MB-231 breast cancer cells in rats (34)[120]	Sunitinib alone, and combination therapy: ↓ (P <0.01)* Zoledronic acid alone: NC	Sunitinib alone, and combination therapy: NC Zoledronic acid alone: NC	Days 5 and 25 in all groups
Sorafenib (multitarget RTK inhibitor) at 7 mg/kg per day ± paclitaxel (mitotic inhibitor; 5 mg/kg per week) or paclitaxel alone	Bone metastases from MDA-MB-231 breast cancer cells in rats (43)[146]	Sorafenib: ↓↓ (P <0.01)* Paclitaxel: ↓ (P <0.01) Combination therapy: ↓↓ (P <0.01)*	Sorafenib: ↓ (P <0.01) Paclitaxel: ↓ (P <0.05) Combination therapy: ↓ (P <0.01)	Day 25 in all groups
Sorafenib 100 mg/kg per day or carmustine (BCNU; alkylating agent; 10 mg/kg every 2 weeks)	U87-MG glioblastoma in rats (60)[102]	Sorafenib: ↓ (P <0.01)* Carmustine: NC	Sorafenib: NC Carmustine: NC	Sorafenib: day 5 Carmustine: days 1–14
MMP inhibition				
Prinomastat (AG-3340); 150 mg/kg twice daily	HaCaT-RAS-A-5RT3 human skin carcinoma in mice (14)[149]	↓ (P <0.05)*	NC	Day 6
VEGF inhibition				
Bevacizumab; 10 mg/kg per week	Human glioblastoma spheroids in rats (8)[183]	↓ (P <0.05)*	NC	Day 21
Bevacizumab; 25 mg/kg every 2 days	U87-MG glioblastoma in mice (6)[139]	NC	↓ (P <0.01)	Days 14 and 22
Bevacizumab; 1 mg every 3 days	HaCaT-RAS-A-5RT SCC in mice (16)[144]	NC	NC	Day 6
Bevacizumab (5 mg/kg every 4 days) ± irinotecan (topoisomerase 1 inhibitor; 40 mg/kg per week)	U87-MG glioblastoma in rats (16)[145]	Bevacizumab: ↓ (P <0.05)* Combination therapy: ↓ (P <0.05)*	Bevacizumab: NC Combination therapy: NC	Day 16 in both groups

Treatment approach	Cancer model (number of animals)	Change in microvessel calibres	Change in macrovessel calibres	Time of response after therapy
G6-31; single 5 mg/kg dose	HM7 CRC in mice (9)[119]	NC	↓ (P <0.01)	Day 2
Neuropilin-1 (NRP1); single 80 mg/kg dose	HM7 CRC in mice (10)[119]	NC	↓ (P <0.05)	Day 2
VEGFR inhibition/antagonism				
Cediranib (AZD2171; 3–6 mg/kg per day)	U87-GFP glioblastoma in mice (24)[148]	↓↓ (P <0.05)*	↓ (P <0.01)	Days 2–3
Vatalanib (PTK787); 75 mg/kg per day	H1975 NSCLC in mice (12)[154]	NC	NC	Days 6 and 13
Tandutinib (MLN518; VEGFR inhibitor) at 20 mg/kg twice daily	C6 glioma in mice (30)[156]	NC	NC	Day 10
DC101 (anti-VEGFR2 antibody); 800 μg per day	HaCaT-RAS-A-5RT3 human skin carcinoma in mice (7)[147]	↓ (P <0.01)*	NC	Day 7
Vascular disruption				
Vadimezan (DMXAA, ASA404); 350 mg/kg per day	GH3 prolactinoma in rats (12)[138]	↓ (P <0.01)	↓ (P <0.01)	Day 1
Vadimezan (DMXAA, ASA404); 350 mg/kg per day	Orthotopic glioma in rats (6)[153]	NC	NC	Day 1
Zybrestat (CA4P); single 50 mg/kg dose	C3H mammary carcinomas in mice (43)[140]	↓ (P <0.01)	↓ (P <0.01)	3 h
ZD6126; 200 mg/kg per day	PC3LN3 prostate carcinoma in mice (6)[143]	↓ (P <0.05)	↓ (P <0.05)	Day 1
ZD6126; 30 mg/kg or 200 mg/kg per day	SW1222 CRC in mice (15)[62]	30 mg/kg: NC 200 mg/kg: ↓ (P <0.05)	30 mg/kg: NC 200 mg/kg: ↓ (P <0.05)	Day 1 for both groups
Src kinase inhibition				
Saracatinib (AZD0530); 25 mg/kg per day	PC3LN3 prostate carcinoma in mice (14)[155]	NC	NC	Day 5
PI3K/mTOR inhibition				
GDC-0980; 10 mg/kg per day	HM7 CRC in mice (18)[184]	↓ (P <0.01)*	NC	Day 1

*An apparent increase in mVD and VSI was observed because of the larger decrease in microvessel calibres compared with macrovessel calibres.

↓, Significant reduction; ↓↓, larger relative decrease in microvessel (radius <10 μm) or macrovessel calibres (total blood volume).

Abbreviations: BCNU, bischloroethylnitrosourea; CRC, colorectal carcinoma; FLT3, FMS-like tyrosine kinase-3; MMP, matrix metalloproteinase; mTOR, mammalian target of rapamycin; NC, no change; NR, not reported; NSCLC, non-small-cell lung carcinoma; PI3K, phosphatidylinositol 3-kinase; RTK, receptor tyrosine kinase; SCC, squamous-cell carcinoma; VEGF, vascular endothelial growth factor; VEGFR(2), VEGF receptor (2).